

Deep Generative Models on 3D Representations: A Survey

Zifan Shi*, Sida Peng*, Yinghao Xu*, Yiyi Liao, and Yujun Shen

Abstract—Generative models, as an important family of statistical modeling, target learning the observed data distribution via generating new instances. Along with the rise of neural networks, deep generative models, such as variational autoencoders (VAEs) and generative adversarial network (GANs), have made tremendous progress in 2D image synthesis. Recently, researchers switch their attentions from the 2D space to the 3D space considering that 3D data better aligns with our physical world and hence enjoys great potential in practice. However, unlike a 2D image, which owns an efficient representation (*i.e.*, pixel grid) by nature, representing 3D data could face far more challenges. Concretely, we would expect an ideal 3D representation to be capable enough to model shapes and appearances in details, and to be highly efficient so as to model high-resolution data with fast speed and low memory cost. However, existing 3D representations, such as point clouds, meshes, and recent neural fields, usually fail to meet the above requirements simultaneously. In this survey, we make a thorough review of the development of 3D generation, including 3D shape generation and 3D-aware image synthesis, from the perspectives of both algorithms and more importantly representations. We hope that our discussion could help the community track the evolution of this field and further spark some innovative ideas to advance this challenging task.

Index Terms—Generative modeling, 3D representations, deep learning, unsupervised learning, 3D vision.



1 INTRODUCTION

THE rapid development of deep learning [1] has significantly advanced many tasks in the field of computer vision, *e.g.*, visual object recognition [2], [3], object detection [4], [5], [6], image rendering [7], [8], [9], *etc.*, and facilitated our daily life in many aspects, like autonomous driving [10], [11], biological research [12], and intelligent creation [13], [14]. Among all types of techniques, generative modeling [15], [16], [17] plays an important role in data analysis and machine learning. Unlike discriminative models that directly make predictions about the inputs, generative models aim to reproduce the data distribution via creating new instances. For such a purpose, they are required to characterize the data comprehensively. For example, a detection model could ignore the task-irrelevant information (*e.g.*, color) without sacrificing the performance, but a generative model is expected to manage every single detail (*e.g.*, object arrangement as well as the texture of each object) of the image for a satisfying generation. From this perspective, learning a generative model is usually more challenging yet facilitates a range of applications [14], [18], [19], [20].

The past few years have witnessed incredible success of deep generative models [15], [16], [17] in 2D image

synthesis [14], [21], [22]. Despite the different formulations, variational autoencoders (VAEs) [16], autoregressive models (ARs) [23], normalizing flows (NFs) [24], generative adversarial networks (GANs) [15], and the very recent diffusion probabilistic models (DPMs) [17] are all capable of converting a latent variable to a high-quality image. Nowadays, however, learning generative models in the 2D space starts to fail to meet the demand of some real-world applications as our physical world is actually under the 3D space. Taking the film industry as an example, we expect to design 3D digital assets instead of simply producing 2D images to bring an immersive experience. Existing content creation pipelines usually require considerable expertise and human efforts, which could be time-consuming and expensive. Many pioneering attempts [25], [26], [27], [28], [29], [30] have been made to investigate how to generate 3D data¹ automatically, but this kind of studies is still at its early stage.

One of the key differences between 2D generation and 3D generation is the data format. Concretely, a 2D image can be naturally formulated as an array of pixel values, which can be conveniently processed by neural networks [2], [3]. Instead, there are many 3D representations to depict a 3D instance, such as point clouds [31], [32], meshes [33], [34], voxel grids [35], [36], multi-plane images [37], implicit neural representations [9], *etc.* Each representation has its own advantage and limitation. For instance, meshes compactly represent 3D shapes yet are hard to analyze and generate by neural networks due to the irregular data structure. In contrast, voxel grids regularly locate in 3D space and work well with standard convolutional neural

- Z. Shi is with the Department of Computer Science and Engineering, the Hong Kong University of Science and Technology, Hong Kong SAR.
- S. Peng is with the State Key Lab of CAD&CG, College of Computer Science, Zhejiang University, China.
- Y. Xu is with the Department of Information Engineering, the Chinese University of Hong Kong, Hong Kong SAR.
- Y. Liao is with the College of Information Science & Electronic Engineering, Zhejiang University, China.
- Y. Shen is with Ant Group, China.

* denotes equal contribution. This work was done when Zifan Shi, Yinghao Xu were interns at Ant Group.

1. Here, we consider 3D-aware image synthesis as a special case of 3D data even the final output is 2D image.

networks, however, voxel grids are memory-consuming and have difficulty in representing high-resolution 3D scenes. Choosing an adequate representation is therefore crucial to 3D content generation.

Considering the fast-growing of 3D generative models, this paper offers an all-around survey of this field to help the community track its evolution. We would like to mention that there are already some surveys in the literature investigating generative models [38], [39], 3D vision [40], [41], [42], [43], as well as generation of 3D structures [44] and faces [45], but a comprehensive review of 3D generation is still missing. As discussed above, to accomplish such a challenging task, there are many candidate algorithms (*e.g.*, VAEs and GANs) and representations (*e.g.*, point clouds and implicit neural representations) to choose from. This survey helps untangle how different types of generative models are applicable to different representations. We organize the rest of this paper as follows. Sec. 2 clarifies the scope of this survey. Sec. 3 introduces the fundamentals of the 3D generation task, including formulations of various generative models and popular 3D representations. Sec. 4 and Sec. 5 summarize existing approaches for 3D shape generation and 3D-aware image synthesis, respectively. Sec. 6 discusses the downstream applications of 3D generative models. Sec. 7 provides the future work in the 3D generation field.

2 SCOPE OF THIS SURVEY

In this survey, we focus on approaches that train networks to model the data distributions of target 3D samples and support the sampling for the synthesis of 3D representations. We also include methods that predict the conditional probability distribution based on certain inputs, such as image, partial point cloud, or text sentences. Note that these conditional generative methods aim to synthesize 3D representations that respect the inputs while keeping the generation diversity. This is in contrast to classical 3D reconstruction methods that establish one-to-one mapping from the inputs to the target 3D representations. We refer readers to [40], [46] for a review on such approaches. Although our survey includes methods that generate 3D representations for rendering, we do not fully cover the neural rendering methods, which are thoroughly discussed in [40], [47]. This survey is complementary to existing surveys that are related to generative models [38], [39], [44].

3 FUNDAMENTALS

3.1 Deep Generative Models

Generative models aim to learn the actual data distribution in an unsupervised manner by trying to produce data as realistically as possible from the given information, which captures more details and shows more creativity. Specifically, generative models are first required to summarize the distribution of input data and then leveraged to create or synthesize samples in the given data distribution. In general, generative models can be divided into two main categories. One is likelihood-based models, including variational autoencoders (VAEs) [16], normalizing flows (N-Flows) [24], diffusion models (DDPMs) [17] as well as energy-based models (EBMs) [48], which are learned by

maximizing the likelihood of the given data. The other one is likelihood-free models, including Generative Adversarial Networks (GANs) [15], which are built on a two-player min-max game to find nash equilibrium. In the following, we will briefly review different types of generative models. Fig. 1 shows the general concept of each generative model.

Generative Adversarial Networks. Generative Adversarial Networks, termed GANs, are very popular for data generation owned to their strong performance in data synthesis. Typically, it consists of two separate networks: a generator $G(\cdot)$ takes a latent code sampled from a prior distribution $\mathbf{z} \sim p_{\mathbf{z}}$ as input to create data and a discriminator $D(\cdot)$ aims to distinguish the real data $\mathbf{x} \sim p_{\mathbf{x}}$ from the synthesized one $G(\mathbf{z})$. In the training process, $G(\cdot)$ is required to synthesize data as realistic as possible to cheat the $D(\cdot)$ to regard that these samples are real while $D(\cdot)$ is trained to label synthesis samples by $G(\cdot)$ as fake and training samples \mathbf{x} as real. These two networks compete with each other and can be formulated into a min-max game (zero-sum game). They are jointly optimized with

$$\mathcal{L}_D = -\mathbb{E}_{\mathbf{x} \sim p_{\mathbf{x}}}[\log(D(\mathbf{x}))] - \mathbb{E}_{\mathbf{z} \sim p_{\mathbf{z}}}[\log(1 - D(G(\mathbf{z})))], \quad (1)$$

$$\mathcal{L}_G = -\mathbb{E}_{\mathbf{z} \sim p_{\mathbf{z}}}[\log(D(G(\mathbf{z})))]. \quad (2)$$

With the rise of deep learning, the two networks of GANs are gradually parametrized by deep neural networks such as DC-GAN [49]. Recently GAN variants like PG-GAN [50], StyleGAN1-3 [51], [52], [53] improve the architectures, which are able to synthesize photo-realistic samples. However, since it is difficult to optimize the two-player game, GANs struggle to train the networks in a stable manner, causing itself easier to non-convergence. Besides, GANs also suffer from mode collapse which the generator map several different latent codes into the same output.

Variational Autoencoders. Deep latent variable models (DLVMs) parametrize the data distribution $\mathbf{x} \sim p_{\theta}$ by neural networks via introducing a latent variables \mathbf{z} with a prior distribution $\mathbf{z} \sim p_{\mathbf{z}}$. The desired parameter θ of DLVMs is difficult to differentiate and optimize because the likelihood $p_{\theta}(\mathbf{x}) = \int p_{\theta}(\mathbf{x}|\mathbf{z})p_{\mathbf{z}}(\mathbf{z})d\mathbf{z}$ we want to maximize is intractable. The Variational Autoencoders (VAEs) turn the intractable posterior inference into a tractable problem by performing an efficient approximation on the intractable posterior with $q_{\phi}(\mathbf{z}|\mathbf{x})$. Concretely, $q_{\phi}(\mathbf{z}|\mathbf{x})$ is parameterized with feed-forward model and optimized by minimize the KL divergence between itself and $p_{\theta}(\mathbf{z}|\mathbf{x})$:

$$D_{KL}(q_{\phi}(\mathbf{z}|\mathbf{x})||p_{\theta}(\mathbf{z}|\mathbf{x})) = \log(p_{\theta}(\mathbf{x})) + D_{KL}(q_{\phi}(\mathbf{z}|\mathbf{x})||p_{\theta}(\mathbf{z})) \quad (3)$$

$$- \mathbb{E}_{\mathbf{z} \sim q_{\phi}(\mathbf{z}|\mathbf{x})} \log(p_{\theta}(\mathbf{z}|\mathbf{x})). \quad (4)$$

The log likelihood $\log(p_{\theta}(\mathbf{x}))$ can be re-written into the following form:

$$\log(p_{\theta}(\mathbf{x})) = D_{KL}(q_{\phi}(\mathbf{z}|\mathbf{x})||p_{\theta}(\mathbf{z}|\mathbf{x})) - D_{KL}(q_{\phi}(\mathbf{z}|\mathbf{x})||p_{\theta}(\mathbf{z})) \quad (5)$$

$$+ \mathbb{E}_{\mathbf{z} \sim q_{\phi}(\mathbf{z}|\mathbf{x})} \log(p_{\theta}(\mathbf{z}|\mathbf{x})) \quad (6)$$

$$\geq -D_{KL}(q_{\phi}(\mathbf{z}|\mathbf{x})||p_{\theta}(\mathbf{z})) + \mathbb{E}_{\mathbf{z} \sim q_{\phi}(\mathbf{z}|\mathbf{x})} \log(p_{\theta}(\mathbf{z}|\mathbf{x})) \quad (7)$$

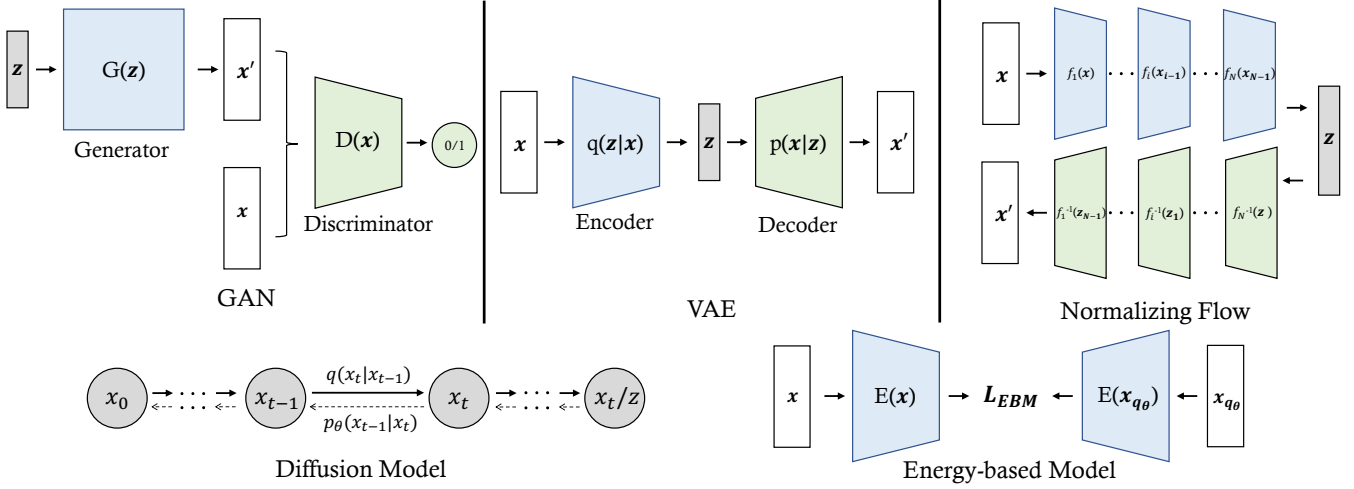


Fig. 1. An overview of different generative models.

where the term $D_{KL}(q_\phi(\mathbf{z}|\mathbf{x})||p_\theta(\mathbf{z}|\mathbf{x}))$ can be eliminated since KL divergence is always non-negative. The above defines the loss function of VAE:

$$\mathcal{L}_{VAE} = -D_{KL}(q_\phi(\mathbf{z}|\mathbf{x})||p_\theta(\mathbf{z})) + \mathbb{E}_{\mathbf{z} \sim q_\phi(\mathbf{z}|\mathbf{x})} \log(p_\theta(\mathbf{z}|\mathbf{x})) \quad (8)$$

which is named as evidence lower bound (ELBO) [54]. To optimize this objective function, [16] also proposes the reparameterization trick to make the process of generating samples $\mathbf{z} \sim q_\phi(\mathbf{z}|\mathbf{x})$ differentiable. Thanks to the feed-forward mode of $q_\phi(\mathbf{z}|\mathbf{x})$, it is efficient to infer new samples. And the training process is stable because of the reconstruction-based loss function. However, VAEs also suffer from the posterior collapse, where the learned latent space becomes uninformative to reconstruct the given data. Because of the injected noise and imperfect reconstruction, VAEs are more likely to synthesize much more blur samples than those coming from GANs.

Normalizing Flows. GANs and VAEs use parametrized models to implicitly learn the density of data so that they can't calculate the exact likelihood function to optimize the model training. Normalizing flows alleviate this problem by introducing a set of invertible transformation functions. Specifically, it starts from a normal distribution, and a set of the invertible function $f_{1:N}(\cdot)$ sequentially transforms the normal distribution to the probability distribution of the final output:

$$\mathbf{z}_i = f_{i-1}(\mathbf{z}_{i-1}). \quad (9)$$

Owing to the invertible properties of the f_i , the probability density function of the new variable \mathbf{z}_i can be easily estimated from the last step \mathbf{z}_{i-1} :

$$p(\mathbf{z}_i) = p(\mathbf{z}_{i-1}) \left| \frac{d\mathbf{f}_i}{d\mathbf{z}_{i-1}} \right|^{-1}, \quad (10)$$

$$\log p(\mathbf{z}_i) = \log p(\mathbf{z}_{i-1}) - \log \left| \frac{d\mathbf{f}_i}{d\mathbf{z}_{i-1}} \right|. \quad (11)$$

And following the chain rule, the density of final output \mathbf{z}_N after N transformations can be obtained by the following:

$$\log p(\mathbf{z}_N) = \log p(\mathbf{z}_0) - \sum_{i=1}^N \log \left| \frac{d\mathbf{f}_i}{d\mathbf{z}_{i-1}} \right|. \quad (12)$$

where the full chain consisting of \mathbf{z}_i is named as normalizing flow. Thanks to the invertible property, normalizing flow can be easily used for novel sample generation, latent variable projection as well as density value estimation. However, it struggles with balancing the parameterized model's capacity and efficiency.

Diffusion Models. Diffusion models [17] is parameterized by a Markov chain, which gradually adds noise to the input data \mathbf{x}_0 by a noise schedule $\beta_{1:T}$ where T denotes the time steps. Theoretically, when $T \rightarrow \infty$, \mathbf{x}_T is a normal Gaussian distribution.

$$q(\mathbf{x}_t|\mathbf{x}_{t-1}) = \mathcal{N}(\mathbf{x}_t; \sqrt{1 - \beta_t}\mathbf{x}_{t-1}, \beta_t\mathbf{I}), \quad (13)$$

$$q(\mathbf{x}_{1:T}|\mathbf{x}_0) = \prod_{t=1}^T q(\mathbf{x}_t|\mathbf{x}_{t-1}). \quad (14)$$

And then, the reverse of the diffusion process is learned to reconstruct the input by modeling the transition $q(\mathbf{x}_{t-1}|\mathbf{x}_t)$ from the noise to the data. However, the posterior inference $q(\mathbf{x}_{t-1}|\mathbf{x}_t)$ is also intractable so that a parametric model p_θ is used to model the conditional transition probability by optimizing the ELBO like VAEs. Because of the intractable long Markov chain, diffusion can synthesize high-quality data and is trained in a stable manner. However, it is expensive to infer new samples, and the sampling process is slower than GANs and VAEs.

Energy-based model. Energy-based models leverages the energy function to explicitly model the probability distribution of data. It is built upon a fundamental idea that any probability function can be transformed from a energy function by dividing its volume:

$$p(\mathbf{x}) = \frac{\exp(-E_\theta(\mathbf{x}))}{\int_{\mathbf{x}} \exp(-E_\theta(\mathbf{x}))}, \quad (15)$$

where $-E_\theta(\mathbf{x})$ is the energy function. Obviously, data points with high likelihood have a low energy, while data

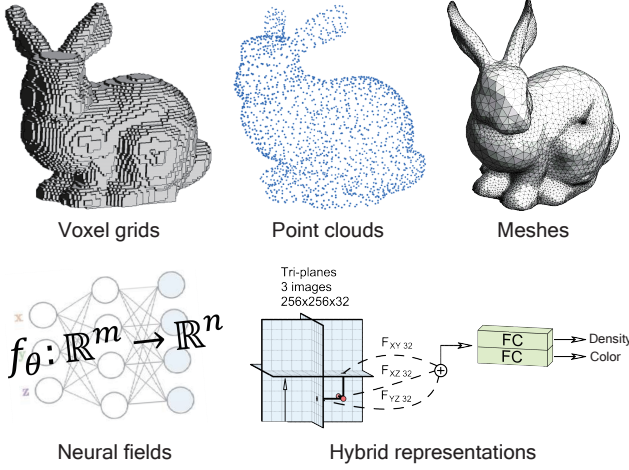


Fig. 2. An overview of 3D representations. Images adapted from [43], [55], [56], [57].

points with low likelihood have a high energy. However, it is difficult to optimize the likelihood because calculating $\int_{\mathbf{x}} \exp(-E(\mathbf{x}))$ for high-dimensional data is intractable. Contrastive divergence is proposed to alleviate the optimization difficulty by compare the likelihood gradient on $p(\mathbf{x})$ and randomly sampled data of energy distribution $q_{\theta}(\mathbf{x})$:

$$\nabla_{\theta} \mathbb{E}_{\mathbf{x} \sim q_{\theta}} (-\log(p(\mathbf{x}))) = \quad (16)$$

$$= \mathbb{E}_{\mathbf{x} \sim p} ((E_{\theta}(\mathbf{x}))) - \mathbb{E}_{\mathbf{x} \sim q_{\theta}} ((E_{\theta}(\mathbf{x}))) \quad (17)$$

The energy distribution $q_{\theta}(\mathbf{x})$ is approximated by Markov Chain Monte Carlo (MCMC) process.

3.2 3D Representations

The computer vision and computer graphics communities have developed various 3D scene representations, including voxel grids, point clouds, meshes, and neural fields. These representations exhibit their own pros and cons in the tasks of 3D shape generation and 3D-aware image synthesis. For example, in contrast to well-structured 2D images, most 3D representations are not in a regular format and cannot be directly processed with standard CNNs. 3D voxel grids are typically regular, enabling it to work well with 3D convolutional networks. However, voxel grids tend to be memory-consuming and thus have difficulty in representing shapes of high resolution. Neural fields theoretically support high-resolution shape modeling, but the effective supervision on implicit representations during training is a problem to be solved.

In the following, we will introduce the formulations of the widely used 3D representations and their representative work, which provides the background for the in-depth analysis of these representations in 3D generation tasks. An overview of 3D representations is available in Fig. 2.

Voxel grids. Voxels are Euclidean-structured data that are regularly placed in 3D space, which is similar to pixels in 2D space. To represent 3D shapes, voxels can store the geometry occupancies [35], [36], volume densities [58], [59], or signed distance values [60]. Thanks to the regularity of

voxel grids, they work well with standard convolutional neural networks and are widely used in deep geometry learning. As a pioneer, 3D ShapeNets [35] introduces voxel grids into 3D scene understanding tasks. It converts a depth map into a 3D voxel grid, which is further processed by a convolutional deep belief network. Instead of being network inputs in aforementioned methods, voxel grids are often used as the network output in the task of 3D reconstruction [61]. 3D-R2N2 [61] uses 2D CNNs to encode the input image into the latent vector and utilizes a 3D convolutional neural network to predict the target voxel grid. Although voxel grids are well suited to 3D CNNs, processing voxels with neural networks is typically memory inefficient. To overcome this problem, [62], [63], [64], [65] introduce the octree data structure for shape modeling.

Voxel grids also have many applications in rendering tasks. Early methods [66], [67] store high-dimensional feature vectors at voxels to encode the scene geometry and appearance, which are typically called feature volumes and can be interpreted into color images using projection and 2D CNNs. Neural Volumes [68] uses CNNs to predict RGB-Alpha volumes and synthesizes images with volume rendering techniques [69]. Multi-plane image (MPI) [37] can be seen as a type of voxel grid, which divides the 3D space into a few depth planes and defines rgb-alpha images at these depth planes. Since they reduce the number of voxels along the depth dimension, MPI-based methods save the computational cost to some extent. Recently, there is a trend in combining voxel grids with neural fields, which is discussed in the section of hybrid representations.

Point clouds. A point cloud is an unordered collection of points in 3D space (Depth and normal maps can be considered as a special case of point cloud representation). It can be seen as discretized samples of a 3D shape surface. Point clouds are the direct outputs of depth sensors, so they are very popular in 3D scene understanding tasks. Although they are convenient to obtain, the irregularity of point clouds makes them difficult to be processed with existing neural networks that are for regular grid data (e.g., images). Moreover, the underlying 3D shape could be represented by many different point clouds due to the sampling variations. Many methods [31], [32], [70], [71], [72], [73] have attempted to effectively and efficiently analyze 3D point clouds. PointNet [31] leverages MLP networks to extract feature vectors from point sets and summarizes features of all points via max-pooling for point order invariance. PointNet++ [32] hierarchically groups the point clouds into several sets and separately processes local point sets with PointNet, which captures the local context of point clouds at multiple levels. Some methods reformulate point clouds as other types of data structures and attempt to exploit neural networks in other fields. DGCNN [72] regards point clouds as graphs and aims to model the relationships among neighboring points using graph CNNs. [73] converts point clouds into sparse voxels and processes them with 3D sparse convolutional networks.

To synthesize images with point clouds, a naive way is storing colors on points and rendering point clouds using the point splatting. Since the rendered images tend to contain holes, [74] uses 2D CNNs to refine images. Some methods [75], [76] have developed differentiable renderers

for point clouds, which can optimize not only for point positions, but also for colors and opacity of points. To increase the modeling capacity of point clouds, [77], [78], [79] attempt to anchor high-dimensional feature vectors to points and project them to feature maps for the latter rendering. Based on this pipeline, ADOP [80] presents a well-developed system that performs free-viewpoint scene navigation in real time. Recent methods [81], [82] try to integrate point clouds with neural fields to achieve high-resolution rendering results, which are discussed in the section of hybrid representations.

Meshes. Polygonal meshes are non-Euclidean data that represent shape surfaces with a collection of vertices, edges and faces. In contrast to voxels, meshes only model scene surfaces and thus are more compact. Compared with point clouds, meshes provide the connectivity of surface points that models the point relationship. Because of these advantages, polygonal meshes are widely used in traditional computer graphics applications, such as geometry processing, animation, and rendering. However, applying deep neural networks to meshes is more challenging than to point clouds because mesh edges need to be taken into consideration in addition to vertices. [33], [83] parameterize 3D shape surfaces as 2D geometry images and process geometry images with 2D CNNs, which avoids handling 3D topology. With the advancement of graph neural networks, [84], [85], [86], [87] propose to regard meshes as graphs. MeshCNN [85] specifically designs convolutional and pooling layers for mesh edges and extracts edge features for shape analysis. As with mesh analysis, generating meshes with networks is also challenging as both vertex position and topology need to be predicted. [34], [88], [89], [90] pre-define a mesh with fixed connectivity and predict vertex displacements to deform the mesh to produce the target shape. To model shapes with more complex topology, [91] proposes a topology modification module that prunes faces of the pre-defined mesh.

In the rendering pipeline of traditional computer graphics, both software and hardware have been heavily optimized for rendering meshes. Some differentiable mesh renderers [92], [93], [94] leverage the advances of classical rendering techniques and design the back-propagation process to update some properties (e.g., colors) defined on meshes. To improve the rendering quality, a strategy is storing appearance properties on shape surfaces, which are parameterized as texture maps. During rendering, UV maps are used to query values at texture maps for arbitrary surface points. Learning-based methods [95], [96] define learnable feature vectors in texture maps, which encode the surface appearance and are decoded into color images with a 2D renderer. Since the features are trained end-to-end from observed images, they are able to learn to compensate the imperfect scene geometry. Recent methods [97], [98] have attempted to improve the mesh representation with neural fields for rendering high-quality images, which are discussed in the section of hybrid representations.

Neural fields. A neural field is a continuous neural implicit representation and represents scenes or objects fully or partially with a neural network. For each position in 3D space, the neural network maps its related features (e.g., coordinate) to the attributes (e.g., an RGB value). Neural fields

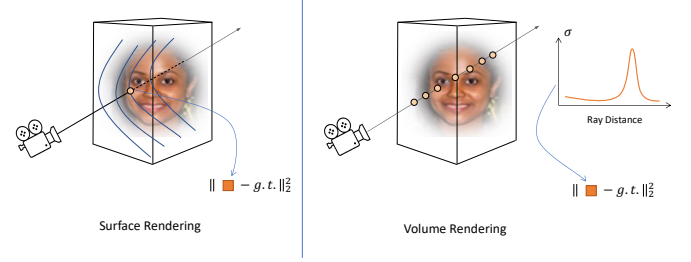


Fig. 3. Surface rendering v.s. volume rendering.

[7], [8], [9], [142], [143], [144], [145] are able to represent 3D scenes or objects in arbitrary resolution and unknown or complex topology due to its continuity in representation. Besides, compared to the aforementioned representations, only the parameters of the neural network are required to store, resulting in lower memory consumption compared to other representations. ONet [142] firstly uses deep neural networks to model the neural fields, where each point in 3D space is mapped to an occupancy value. Differently, DeepSDF [143] uses signed distance values as the attribute of each point in neural fields.

To render an image from a neural field, there are two streams of techniques - surface rendering and volume rendering. Surface rendering [146], [147] employs an implicit differentiable renderer that first shoots viewing rays and finds the intersection points with the surface, as shown in Fig. 3. The RGB values of these intersection points are then queried from the network and form a 2D image. Though surface rendering based methods exhibit good performance on representing 3D objects and rendering 2D images, per-pixel object masks and careful initialization are required by most of them to help optimize to a valid surface. The reason is that surface rendering only provides gradient at the ray-surface intersection points and makes the network hard to optimize. Volume rendering [69], in contrast, is based on ray casting and samples multiple points along each ray, which is shown in Fig. 3. It has shown great power in modeling complex scenes. For each camera ray with origin \mathbf{o} and direction \mathbf{d} , the observed color is

$$\mathbf{C}(\mathbf{o}, \mathbf{d}) = \int_{t_n}^{t_f} T(t, \mathbf{o}, \mathbf{d}) \sigma(\mathbf{o} + t\mathbf{d}) \mathbf{c}(\mathbf{o} + t\mathbf{d}) dt, \quad (18)$$

where t_n and t_f determine the near and far bound of the ray. σ denotes the density of a point and \mathbf{c} is the emitted color of it. The accumulated transmittance value T is defined as follows

$$T(t, \mathbf{o}, \mathbf{d}) = \exp \left(- \int_{t_n}^t \sigma(\mathbf{o} + s\mathbf{d}) ds \right). \quad (19)$$

The aggregated colors from all rays result in a 2D image. NeRF [9] and its following works adopt such differentiable volume rendering to render 2D images from 3D representations, allowing gradients to flow through the renderer. However, sampling a set of points along all rays may lead to low rendering speed. Recent works focus on acceleration via various techniques, such as pruning [148], improved integration [149], and carefully-designed data structures [150], [151], [152], [153].

TABLE 1

Properties of representative methods on 3D shape generation. Units for “FLOPS” and “Num. of Params.” are in G and M, respectively. We calculate the two metrics for methods implemented using PyTorch [99]. “Controllability” is described in Section 6.2. “Dataset” indicates which datasets are used for training generative models.

Method	Publication	3D representation	Generative model	FLOPS	Num. of Params.	Shape resolution	Controllability	Dataset
Wu <i>et al.</i> [25]	NeurIPS 2016	Voxel grid	GAN	-	-	-	-	[35], [100]
Brock <i>et al.</i> [101]	arXiv 2016	Voxel grid	VAE	-	-	-	-	[35]
SAGNet <i>et al.</i> [102]	TOG 2019	Voxel grid	VAE	-	-	-	Part-level	[102]
Guan <i>et al.</i> [103]	CVPRW 2020	Voxel grid	VAE	-	-	-	-	[35], [104]
PQ-Net [105]	CVPR 2020	Voxel grid	VAE	0.02	13.62	$64 \times 64 \times 64$	Part-level	[106]
Generative VoxelNet [107]	TPAMI 2020	Voxel grid	Energy-based model	-	-	-	-	[35]
AutoSDF [60]	CVPR 2022	Voxel grid	VQ-VAE	997.41	2941.10	$64 \times 64 \times 64$	-	[108]
Achlioptas <i>et al.</i> [26]	ICML 2018	Point cloud	GAN	-	-	-	-	[35], [108], [109]
MRTNet [110]	ECCV 2018	Point cloud	VAE	-	-	-	-	[35], [108]
Shu <i>et al.</i> [111]	ICCV 2019	Point cloud	GAN	-	-	-	-	[108]
PC-GAN [112]	arXiv 2018	Point cloud	GAN	-	-	-	-	[108]
Valsesia <i>et al.</i> [113]	ICLR 2018	Point cloud	GAN	-	-	-	-	[108]
PointFlow [114]	ICCV 2019	Point cloud	Normalizing flow	105.89	1.06	2048	-	[35], [108]
Spectral-GAN [115]	IROS 2020	Point cloud	GAN	-	-	-	-	[35], [108]
Hui <i>et al.</i> [116]	ECCV 2020	Point cloud	GAN	25.79	12.71	2048	-	[35], [108]
Arshad <i>et al.</i> [117]	3DV 2020	Point cloud	GAN	-	-	-	-	[108]
Zamorski <i>et al.</i> [118]	CVIU 2020	Point cloud	VAE	0.01	7.03	2048	-	[35], [108]
ShapeGF [119]	ECCV 2020	Point cloud	Energy-based model	413.85	4.17	2048	-	[108], [120]
SoftFlow [121]	NeurIPS 2020	Point cloud	Normalizing flow	5.26	6.50	2048	-	[108]
DPF-Net [122]	ECCV 2020	Point cloud	Normalizing flow	-	-	-	-	[108]
PointGrow [123]	WACV 2020	Point cloud	Auto-regressive	-	-	-	-	[35], [108], [124]
SP-GAN [125]	TOG 2021	Point cloud	GAN	1.64	0.59	2048	Part-level	[108], [126], [127]
Generative PointNet [128]	CVPR 2021	Point cloud	Energy-based model	91.86	1.39	2048	-	[35]
Luo <i>et al.</i> [129]	CVPR 2021	Point cloud	Diffusion model	67.33	3.30	2048	-	[35], [108]
PolyGen [130]	ICML 2020	Mesh	Auto-regressive model	-	-	-	-	[108]
TM-Net [131]	TOG 2021	Mesh	VAE	-	-	-	Part-level	[108]
Ben-Hamu <i>et al.</i> [132]	TOG 2018	Mesh	GAN	-	-	-	-	[109], [133]
IM-Net [27]	CVPR 2019	Neural field	GAN	799.70	3.05	$256 \times 256 \times 256$	-	[108]
Kleineberg <i>et al.</i> [134]	arXiv 2020	Neural field	GAN	7726.65	0.46	$256 \times 256 \times 256$	-	[108]
DualSDF [135]	CVPR 2020	Neural field	Auto-decoder	-	-	-	Part-level	[108]
Ibing <i>et al.</i> [136]	CVPR 2021	Neural field	Auto-decoder	-	-	-	-	[108]
Deng <i>et al.</i> [137]	CVPR 2021	Neural field	Auto-decoder	209.11	0.10	$256 \times 256 \times 256$	-	[138]
gDNA [139]	CVPR 2022	Neural field	Auto-decoder	425.90	0.87	$256 \times 256 \times 256$	-	[140]
ShapeAssembly [141]	TOG 2020	Program	VAE	0.02	1.41	-	Part-level	[106]

Hybrid representation. Considering the pros and cons of each representation, hybrid representations are proposed to complement each other. Most of the hybrid representations focus on the combination of explicit and implicit representations. Explicit representations provide explicit control over the geometry. On the other hand, they are restricted by the resolution and topology. Implicit representations enable modeling complex geometry and topology with relatively small memory consumption. However, they are usually parameterized with MLP layers and output the attribute for each coordinate, suffering from small receptive fields. Thus, they are difficult to give explicit supervision on surfaces and hard to optimize. Researchers leverage the advantages of each type of representations to make up for the shortcomings of the other type of representations.

Some works [148], [151], [154] integrate voxel grids into neural fields to accelerate the learning and rendering. The features of points for differentiable rendering are interpolated from the features of voxel grids. These representations sacrifice memory consumption for rendering speed. MINE [155] merges neural fields with multi-plane images, which is a smaller representation than voxel grids but suffers from limited viewing range. EG3D [57] uses tri-planes to boost the model capacity of neural fields. Such representations consume less memory than voxel-based neural fields, and they allow fast rendering at the

same time. [156] and [82] build a neural field on a point cloud, which can be seen as an unordered version of voxel-based neural fields. [156] interpolates point features from K neighboring points. [82] uses a hyper-network that takes in a point cloud and then generates the weights of NeRF network. NeuMesh [98] presents mesh-based neural fields by encoding geometry and texture codes on mesh vertices, enabling manipulation on neural fields through meshes. [97], in contrast, combines two explicit representations, mesh and voxel grids. The proposed deformable tetrahedral meshes representation optimizes both the vertex placement and occupancy. Thus, the surfaces are inherently represented by tetrahedral meshes, and this representation achieves both memory and computation efficiency. Hybrid representations seek to maximize the benefits of utilizing various representations. Hence, they are attracting more and more attention.

4 3D SHAPE GENERATION

Recently, most of 3D shape generation methods train deep neural networks to capture the distribution of 3D shapes. In contrast to 2D images, 3D shapes have many types of representations, such as voxel grids, point clouds, meshes, and neural fields. These representations exhibit their own advantages and disadvantages in the task of 3D shape

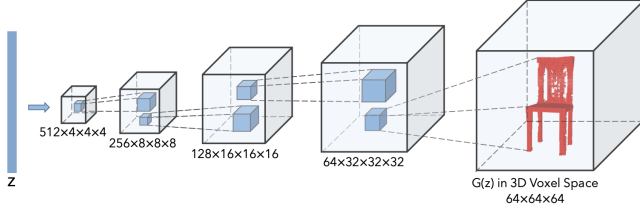


Fig. 4. Wu *et al.* [25] generate 3D shapes with standard 3D convolutional neural networks. Image adapted from [25].

generation. There are many aspects that can be considered to evaluate whether the 3D representation can work well with deep generative models, including the ease of network processing on the representation, the allowance of efficient generation of high-quality and complex 3D shapes, and the cost of obtaining supervision signals for generative models. Tab. 1 summarizes the representative methods on 3D shape generation.

4.1 Voxel Grids

Voxel grids are usually seen as images in the 3D space. To represent 3D shapes, voxels could store the geometry occupancy, signed distance values or density values, which are implicit surface representations that define the shape surface as a level-set function. Thanks to the regularity of its data structure, voxel grid is one of the earliest representations being used in deep learning techniques for 3D vision tasks, such as 3D classification [35], [36], [101], 3D object detection [157], [158], and 3D segmentation [159], [160].

Wu *et al.* [25] adopt the architecture of generative adversarial networks to process 3D voxel grids. As illustrated in Fig. 4, the generator maps a high-dimensional latent vector to a 3D cube, which describes the synthesized object in voxel space. Different from 2D GANs, the generator and discriminator are built with a series of 3D convolution blocks to make the GAN process the 3D voxel data. In practice, they also build an encoder to project the 2D image into the latent space of its generator, which is similar to VAE-GAN [161]. So besides the conventional adversarial loss, it also consists of two parts for the encoder training: a reconstruction loss and a KL divergence loss to constrain the output distribution of the encoder. Owing to its VAE-GAN-like design, this model can also be leveraged to recover 3D shapes from the 2D observation. They also demonstrate that the discriminator learned without any supervision can be successfully transferred to several 3D downstream tasks with good performance. Considering the training of GAN models is unstable, [101] attempts to train a variational auto-encoder to model the shape distribution, as shown in Fig. 5. It first uses an encoder network consisting of four 3D convolutional layers and a fully connected layer to map the input voxel into a latent vector and then the 3D decoder with an identical but inverted architecture to transform a latent vector into a 3D voxel. The downsampler in the encoder and upsampler in the decoder are implemented by stride convolutions. The objective function for training consists of two parts: one is KL divergence on the latent codes, and the other

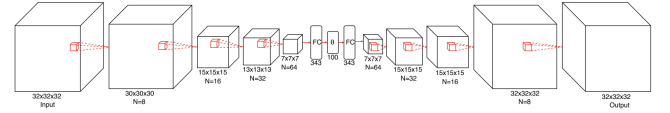


Fig. 5. Brock *et al.* [101] adopt the variational auto-encoder framework for 3D shape generation. Image adapted from [101].

is a Binary Cross-Entropy (BCE) for voxel reconstruction. They adjust modifications to the BCE loss to avoid gradient vanishing. Even though this method can handle dense objects, it suffers from producing smooth rounded edges, which is similar to 2D VAE, tending to generate blurry voxels. To solve these problems, [60] introduces VQ-VAE to model the data distribution. Different from VAE, only using a single vector serving as a latent for input, they use VQ-VAE to project the high-dimensional 3D shape into a lower-dimensional discrete latent space which is optimized during training, not fixed like VAE. Once the latent space is well trained, they use a transformer to autoregressively model the non-sequential data. Specifically, they maximize the likelihood of the latent representations using randomized orders for an autoregressive generation. And the well-trained autoregressive model can be used for various downstream applications, including shape completion, and text-guided shape generation, which is simply achieved by fusing conditional information to the autoregressive model.

In addition to modeling the whole object shape, some works attempt more fine-grained shape generation. [102] proposes to use an autoencoder to jointly learn the geometry of the part and the pairwise relationship between different parts. It uses two-way encoder to separately extract the features of the geometry and structure. And GRU and attention modules are also incorporated into the encoder to exchange the geometry and structural information encoded by two independent encoders and summarize the input into a latent code. And a two-way decoder is introduced to decode the input geometry and structure. Because of modeling the structure and geometry explicitly, it can enable the disentangling control of the geometry and the structure. [162] also proposes to model 3D shape variations at part-level. However, they also pay attention to how to automatically assemble different parts into a whole 3D shape. Specifically, it first learns a part-wise generative network, consisting of K part generator where K is the number of the parts. The part generator is built up on 3D VAE-GAN, which is very similar to [25] but the difference is they also introduce a reflective symmetry loss to prevent generating asymmetric parts because most parts of the datasets [108] are reflective symmetric. To assemble the synthesized parts with different scales and positions, it introduces a part assembler to regress the transformation for the individual part, which is used to compose parts into a complete shape volume. Since the assembling solution is not unique for the given parts, they propose to set a fixed anchor part while the remains are required to learn the transformation to match the anchor part. At the inference stage, they can generate shapes by sampling the latent space, and the assembling model can compose different parts automatically. [105] also firstly encodes each part by a geometry autoencoder and

then uses a sequence-to-sequence (Seq) for part assembly. Thanks to the Seq2Seq modeling, the decoder can perform very well for several tasks, including shape generation and single-view 3D reconstruction.

Although the above approaches can perform well with a low-resolution voxel as inputs, it cannot handle fine-grained voxel with a large resolution because the computation cost grows cubically. To alleviate these issues, [163] tries to use octree as a hierarchical compact representation for the voxel grid and then convert the octree into sequence by traversal ordering. Besides, an adaptive compression scheme used to decrease the sequence length can also improve the efficiency with a transformer-based generator.

Voxel grids like 2D images, are in a euclidean structure, which works well with 3D CNNs. However, the voxel grid consumes much computation cost because the number of voxel elements grows cubically with resolution and quickly become intractable already at low resolutions. In contrast, octree for voxel can reduce a lot of computation, but due to its non-grid structure, it cannot be processed by neural network very efficiently.

4.2 Point Clouds

Since point clouds are direct outputs of depth scanners, they are a popular representation in scene understanding tasks. Modeling data priors of certain point cloud datasets with generative models facilitates downstream computer vision tasks [112], [164]. In contrast to voxel grids, point clouds are an explicit surface representation and directly characterize shape properties, which has two advantages. First, deep neural networks usually process point clouds with fewer GPU memory. Second, they are suitable to some generative models, such as normalizing flows and diffusion models. Despite the two advantages, the irregularity of point clouds makes networks difficult to analyze and generate them.

As the pioneer work, Achlioptas *et al.* [26] exploit generative adversarial networks to learn the distributions of 3D point clouds. It proposes a raw point cloud GAN (r-GAN) and a latent-space GAN (l-GAN). The generator of the r-GAN is an MLP network with 5 fully connected layers, which maps the randomly sampled noise vector to the point cloud with 2048 points. The corresponding discriminator uses PointNet [31] as the network backbone. [26] found that r-GAN has difficulty in generating high-quality point clouds. A plausible reason is that GANs are hard to converge to a good point. To overcome this problem, [26] presents a novel training framework that first trains an auto-encoder network and then train a generative adversarial network to model the learned latent space of the auto-encoder, which is called l-GAN. The l-GAN delivers much better performance than r-GAN. The GAN generator of point clouds is typically implemented as fully-connected networks, which cannot effectively leverage local contexts for producing point clouds. To solve this problem, some methods [111], [113], [116], [117] propose to construct the GAN generator based on the graph convolution. For example, given a sampled latent vector, Valsesia *et al.* [113] first use an MLP network to predict a set of point features, which is taken as a graph and processed by a graph convolutional network. When upsampling the point

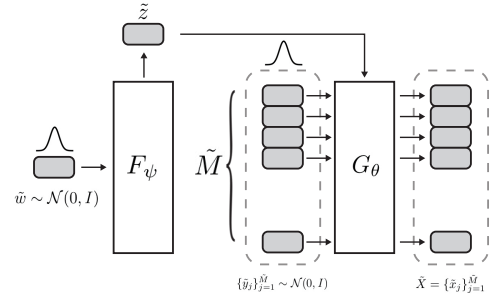


Fig. 6. PointFlow [114] models point clouds as a distribution of distributions and learns the 3D data prior with normalizing flows. Image adapted from [114].

cloud, it applies the graph convolution to point features to obtain new feature vectors, which are concatenated to the original point features to produce the upsampled point set. Another challenge of point cloud generation is that synthesizing high-resolution point clouds easily consumes a lot of memory. Ramasinghe *et al.* [115] reduce the computational complexity by adopting a GAN model in the spectral domain. It represents point clouds as spherical harmonic moment vectors and regresses these vectors from sampled latent vectors with MLP networks.

Although GAN-based methods have produced impressive generation performance, the unstable training drives researchers to explore other types of generative models. [118] extends variational auto-encoder model (VAE) and adversarial auto-encoder model (AAE) to the 3D domain. The encoder is implemented as a PointNet-like network, and the decoder is an MLP network. Since point clouds are irregular, the reconstruction loss for the auto-encoder is implemented as set-to-set matching loss, such as Earth Mover’s distance and Chamfer distance. Same as 2D VAE model, 3D VAE model supervises the latent space with the KL divergence. Considering the KL divergence could be intractable, AAE model instead learns the latent space with the adversarial training. [118] empirically finds that 3D AAE model gives better performance than 3D VAE model.

Due to the non-Euclidean data structure of point clouds, the GAN-based and AE-based generative models mostly use MLP networks or graph convolutional networks to map latent vectors to point clouds, which can typically produce a fixed number of points. This significantly limits their modeling ability. Even for shapes within the same category, their complexity could require different numbers of points. To overcome this problem, PointFlow [114] models point clouds as a distribution of distributions and introduces a normalizing flow model to generate point clouds. Fig. 6 presents its pipeline. Specifically, PointFlow first samples a set of points from a generic prior distribution, such as standard Gaussian. Then, it samples a latent vector from the shape distribution that encodes the shape information and feeds the vector into a conditional continuous normalizing flow (CNF), which produces a vector field to move the sampled points to generate the shape. PointFlow assumes that modeling shape prior as the Gaussian distribution limits the performance of VAE models and thus uses an additional CNF to model the shape prior. Since the Neural

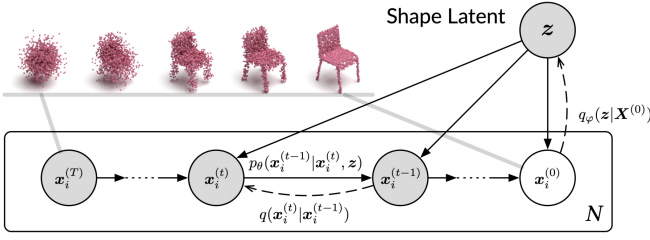


Fig. 7. Luo *et al.* [129] formulate the point cloud generation as a denoising process, which is implemented as a Markov chain. Image adapted from [129].

ODE solver in continuous normalizing flow is computationally expensive, Klovov *et al.* [122] proposes to adopt the affine coupling layers to build discrete normalizing flows, resulting in a significant speedup. Another problem of flow-based models is that they may fail when the dimensions of the data and target distributions are not the same. The point clouds typically lie on 2D manifolds, while a generic prior distribution is defined over the 3D space, making flow-based models struggle to transform point clouds to match the prior distribution. To solve this issue, SoftFlow [121] perturbs point clouds with sampled noise and uses a conditional normalizing flow model to map perturbed points to the latent variables.

Recent methods [119], [129], [165] model the point cloud generation as a denoising process and train a model to output vector fields to gradually move points from a generic prior distribution. ShapeGF [119] regards the shape as a distribution and assumes that points on the shape surface have high densities. For any 3D point, it trains a network to predict the point’s gradient that is used to move the point to the high-density area. [129], [165] formulate the generation of point clouds as reverse diffusion process, which is in contrast to the diffusion process in non-equilibrium thermodynamics. Fig. 7 presents the diffusion process. The reverse diffusion process is implemented as a Markov chain that transforms the distribution of points from the noise distribution to the target distribution. Each transition step is instantiated as an auto-encoder, which takes the point cloud as input and outputs the displacements of points.

PointGrow [123] develops an autoregressive model that recurrently predicts new points conditioned on previously generated points. It designs self-attention modules to capture long-range dependencies. However, the order of points is hard to define. [123] sorts points based on the points’ z coordinates. [128] proposes a deep energy-based model for synthesizing point clouds. The short-run MCMC is adopted as the point generator. The energy model is implemented as a PointNet-like network, which predicts scores for generated point clouds.

Recently, some methods [125], [166] attempt to attain the part-level controllability over the generated shapes. MRGAN [166] proposes a multi-root GAN that consists of multiple branches and each branch map a sampled latent vector to a set of points, which are concatenated into the final point cloud. After training, the parts of generated objects can be edited by revising the corresponding latent vectors. SP-GAN [125] adopt the sphere as prior for the

part-aware shape generation. It defines a fixed point cloud on the unit sphere and anchors the sampled latent vector to each point, which is then fed into a generator to produce the shape. The initial point cloud acts as a guidance to the generative process and provides dense correspondences between generated shapes, naturally enabling the part-level controllability. Changing latent vectors of some points leads to the modification of the associated part.

Point clouds have been adopted in many types of generative models to synthesize shapes. Although previous methods have achieved impressive performance on shape generation, the high-resolution shapes are still difficult to obtain. The reason is that high-resolution shapes requires many points for modeling, which will consume a large amount of GPU memory.

4.3 Neural Fields

Neural fields use neural networks to predict properties for any point in the 3D space. Most of them adopt MLP networks to parameterize 3D scenes and can model shapes of arbitrary spatial resolutions in theory, which is more memory efficient than voxel grids and point clouds. Although neural representations has superiority in the shape modeling, it is not straightforward to apply common generative models such as GANs on these representations, due to the lack of ground-truth data in neural representation format and the difficulty of processing neural representations with neural networks directly. To overcome this problem, some methods use auto-decoders [167] to model the distribution. gDNA [168] adopts an auto-decoder for dynamic human generation. There are two independent latent spaces for detail and shape. A 3D CNN-based feature generator first processes the shape latent code into a feature volume, which is further decoded into occupancy values and feature vectors through an MLP. Surface details are synthesized based on the detail latent code and the decoded features. The learnable 3D transformations are applied on the canonical representations to get the deformed output. [137] aims to preserve shape correspondences when generating shapes. An MLP is used to represent a template implicit field with signed distance function that is shared among all instances. Given a shape code, a deformation field and a correction field are modeled by another two MLPs for each point in the template space. Those points that are deformed from the same point in the template space are considered as correspondences. A SDF regression loss between a collection of shapes and those generated ones is used for training. [135] learns a shared latent space to enable semantic-aware shape manipulation. A sampled latent code will be processed by two networks with representations of different levels of granularity. One is with SDF that can capture fine details while the other one is with simple shape primitives to represent a coarse shape. Two reconstruction losses are calculated between the given shapes and the generated shapes of two representations.

To generate implicit fields based on generative adversarial networks, some methods discriminate the generated implicit fields either in the latent space or with the converted explicit representations. [27] applies the discriminator on the latent space. An auto-encoder is first used to learn the

features from a set of shapes, where the encoder can be a 3D CNN or PointNet [31] while the decoder is parameterized with MLP and takes coordinates and features as input. Then, latent-GANs [26], [169] are employed to train on the features extracted by the pretrained encoder. The generated features can be decoded by the pretrained decoder to get a shape. [136] also leverages latent-GANs but proposes a hybrid representation as the intermediate feature for learning to enable spatial control of the generated shapes. The latent representation combines voxel grids and implicit fields, and therefore each cell covers a part of the shape. [134] outputs SDF values given a coordinate and a latent code in the generator and designs two types of discriminators, voxel-based (*e.g.*, 3D CNN) and point-based (*e.g.*, PointNet). In voxel-based cases, a fixed number of stationary points are fed into the generator and query for SDF value. While in point-based cases, points of arbitrary sequence can be queried for SDF values. SurfGen [170] develops a differentiable operator that extracts surface from implicit fields through marching cubes [171] and then performs differentiable spherical projection on the surface, which is an explicit shape representation. A spherical discriminator operates on the explicit surfaces to supervise the training.

With the development of diffusion models, it is interesting to apply this powerful generative models to learn the distributions of neural fields. [172] starts the initial attempt through representing data using an implicit neural representation and learning a diffusion model directly on the modulation weights of the implicit function. However, blurry results are generated compared to the results from GAN-based methods. Combining neural fields with diffusion models appropriately remains a problem to be explored.

4.4 Meshes and Other Representations

Mesh is one of the most used representations in traditional computer graphics. It is also usually taken as the target object in many 3D modeling and editing softwares. Despite the mesh’s popularity in traditional applications, it is challenging to apply deep generative models to the mesh generation due to two factors. First, meshes are non-Euclidean data and cannot be directly processed by convolutional neural networks. Second, the mesh generation requires to synthesize meshes with plausible connections between mesh vertices, which is difficult to achieve.

To avoid handling the irregular structure of meshes, [132] proposes an image-like representation called multi-chart structure to parametrize the mesh. It defines a set of landmark points on a base mesh, and each triplet of landmark points corresponds to a function that establishes correspondences between a chart on the image domain and the shape surface. By representing meshes with multi-chart structure, [132] can utilize well-developed image GAN techniques to generate shapes. However, the parameterization trick requires the topology of generated meshes similar to the base mesh that used to define the multi-chart structure. To make the generation process easier, SDM-Net [216] registers training meshes with a unit cube mesh, which enables them to have the same connectivity as the template cube mesh. SDM-Net utilizes the variational auto-encoder to learn the distributions of meshes, where the

encoder and decoder are implemented with convolutional operators defined on meshes. Based on [216], TM-Net [131] additionally defines a texture space on the template cube mesh and uses a CNN-based VAE to synthesize texture maps, which are combined with generated meshes to produce textured meshes. PolyGen [130] attempts to synthesize the connectivity of meshes based on an auto-regressive generative model. It develops a transformer-based network to sequentially generate mesh vertices and faces. Similar to PointGrow [123], PolyGen sorted the mesh vertices along the vertical axis and use a vertex transformer for the vertex generation. Then, mesh faces are predicted using a face transformer that is conditioned on generated mesh vertices.

Representing shapes as structured computer programs is an attractive direction. Programs guarantee to produce high-quality geometries and is editable to users. ShapeAssembly [141] proposes to create programs with a VAE model. It turns 3D shapes into programs to construct the training dataset and develops a sequence VAE for learning. To analyze the input program, the encoder uses MLP networks to extract features from each program line and fuse them into a latent vector with a GRU module. During the program generation, the decoder utilizes the GRU to sequentially predict features for each line, which are mapped to the program line using MLP networks.

5 3D-AWARE IMAGE GENERATION

The goal of 3D-aware image generation is to explicitly control the camera viewpoint when synthesizing images. 2D GAN-based models [217], [218], [219], [220], [221] achieve this goal by discovering a latent space direction corresponding to the viewpoint trajectory. Although they deliver impressive results, finding a reasonable direction in the latent space is not easy and usually cannot support the full control of the rendering viewpoint. This survey focuses on works that explicitly generating 3D representations for 3D-aware image synthesis. In contrast to 3D shape generation methods that are directly trained with shapes, most of 3D-aware image generation methods are supervised by images through differentiable neural rendering, because there are typically not high-quality and large-scale datasets of renderable 3D representations for training generative models. Due to the lacking of renderable 3D representations, auto-encoder architectures are barely used in this task. Most methods adopt the generative adversarial model, which samples a latent vector from the latent space and decodes it to the target representation.

Similar to 3D shape generation, there are also several 3D representations commonly used in the task of 3D-aware image generation, including depth/normal maps, voxel grids, and neural fields. Point clouds and meshes are not well explored in generative image synthesis. A reason is that current differentiable neural rendering cannot provides effective gradient signals to optimize these two representations easily. The key factors to be considered when incorporating 3D representation for 2D image generation are quality and efficiency, where the quality includes image realism and view consistency. Representative methods on 3D-aware image generation are summarized in Tab. 2.

TABLE 2

Properties of representative methods on 3D image generation. Units for “FLOPS” and “Num. of Params.” are in G and M, respectively. “Controllability” is described in Section 6.2. “Dataset” indicates which datasets are used for training generative models.

Method	Publication	3D representation	FLOPS	Num. of Params.	Image resolution	Controllability	Dataset
VON [173]	NeurIPS 2018	Voxel grid	-	-	-	Camera pose	[108], [174]
HoloGAN [67]	ICCV 2019	Voxel grid	-	-	-	Camera pose	[108], [175], [176], [177], [178], [179]
BlockGAN [180]	NeurIPS 2020	Voxel grid	-	-	-	Spatial layout	[178], [181]
Wang <i>et al.</i> [182]	ECCV 2016	Normal map	-	-	-	Camera pose	[183]
Noguchi <i>et al.</i> [184]	arXiv 2019	Depth map	-	-	-	Camera pose	[51], [108], [179], [185]
Shi <i>et al.</i> [186]	ECCV 2022	Depth map	63.24	55.81	256 × 256	Camera pose	[179]
Schwarz <i>et al.</i> [28]	NeurIPS 2020	Neural field	177.03	0.68	64 × 64	Camera pose	[50], [176], [177], [187], [188], [189]
Niemeyer <i>et al.</i> [30]	CVPR 2021	Neural field	5.21	0.75	256 × 256	Spatial layout	[50], [51], [177], [178], [179], [187], [189]
Chan <i>et al.</i> [29]	CVPR 2021	Neural field	842.42	1.91	256 × 256	Camera pose	[176], [177], [187]
Pan <i>et al.</i> [190]	NeurIPS 2021	Neural field	1243.66	1.91	256 × 256	Relighting	[175], [176], [177]
Niemeyer <i>et al.</i> [191]	3DV 2021	Neural field	183.86	0.36	128 × 128	Camera pose	[176], [177], [187], [189]
Zhou <i>et al.</i> [192]	arXiv 2021	Neural field	-	-	-	Camera pose	[51], [193]
Xu <i>et al.</i> [194]	NeurIPS 2021	Neural field	621.53	1.91	256 × 256	Camera pose	[175], [176], [177]
Zhang <i>et al.</i> [195]	ECCV 2022	Neural field	-	-	-	Human pose	[196]
Sun <i>et al.</i> [197]	CVPR 2022	Neural field	2094.73	2.70	256 × 256	Semantics	[51], [198]
StyleNeRF [199]	ICLR 2021	Neural field	13.49	7.63	1024 × 1024	Camera pose	[51], [178], [193], [200]
StyleSDF [201]	CVPR 2022	Neural field	-	-	-	Camera pose	[51], [193]
GRAM [202]	CVPR 2022	Neural field	977.91	1.95	256 × 256	Camera pose	[51], [177], [187]
VoLux-GAN [203]	SIGGRAPH 2022	Neural field	-	-	-	Relighting	[51], [176]
GIRAFFE HD [204]	CVPR 2022	Neural field	35366.12	12.78	1024 × 1024	Camera pose	[50], [51], [178], [179], [193]
Zhang <i>et al.</i> [205]	CVPR 2022	Neural field	-	-	-	Camera pose	[50], [51], [193]
Noguchi [206]	arXiv 2022	Neural field	-	-	-	Human pose	[207], [208], [209], [210]
IDE-3D [211]	SIGGRAPH Asia 2022	Neural field	-	-	-	Semantics	[51], [198]
EpiGRAF [212]	arXiv 2022	Neural field	-	-	-	Camera pose	[51], [177]
AvatarGen [213]	arXiv 2022	Neural field	-	-	-	Human pose	[196], [214], [215]
VolumeGAN [58]	CVPR 2022	Hybrid	32.52	8.67	256 × 256	Camera pose	[51], [176], [177], [178], [179], [187]
EG3D [57]	CVPR 2022	Hybrid	25.78	30.60	512 × 512	Camera pose	[51], [193]

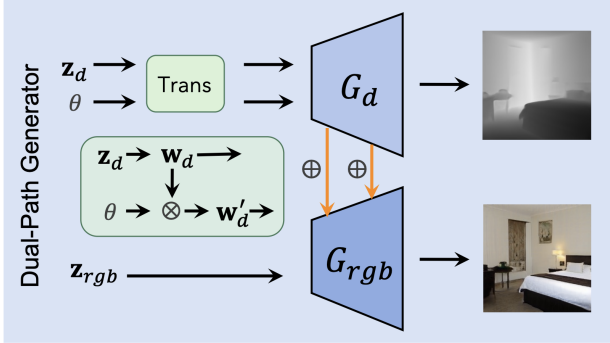


Fig. 8. DepthGAN [186] uses depth images as the scene geometry to enable 3D-aware image synthesis. Image adapted from [186].

5.1 Depth/Normal Maps

Depth and normal maps are easily accessible representations that partially reveal the geometry of 3D scenes or objects. Since they only show the geometry from one side, they are usually referred to as 2.5D representations instead. Depth and normal maps can be involved in image generation with ease (*i.e.*, processed by 2D convolutional neural network rather than 3D architectures) as they share the similar data format as 2D image. Most of methods [182], [184], [186] leverage GAN models to generate depth or normal maps for 3D-aware image synthesis.

S2-GAN [182] proposes to consider the underlying 3D geometry when generating images, where it calls the geometry as structure and the image as style. It develops the Structure-GAN that maps a sampled latent vector to a surface normal map. Then, the normal map is fed into the

Style-GAN with another sampled latent vector to generate the image. The Structure-GAN is implemented as a set of convolution and deconvolution layers, and the Style-GAN is designed based on the conditional GAN [222]. By disentangling the generation of the structure and style, [182] makes the generative process more interpretable and enables the controllability of image synthesis given surface normal maps. To explicitly control the viewpoint of rendered images, RGBD-GAN [184] passes camera parameters into the generator. It assumes RGB and depth image can be generated simultaneously and learns from 2D image data only. To ensure the inter-view consistency of synthesized images, [184] generates two RGBD images under two different viewpoints and warps the RGB-D image from one view to another view to compute the consistency loss. However, the model fails to capture such relationship when the contents in the image become more complex (*e.g.*, bedrooms) and outputs a flat plane. In contrast, [182] and [186] hold the view that appearance should be rendered conditioned on the geometry, where normal maps and depth maps are used, respectively. Similar to S2-GAN [182], DepthGAN [186] develops a dual-path generator for the 3D-aware image synthesis. In contrast to [182] that explicitly conditions the image generation on the synthesized geometry, DepthGAN extracts intermediate features from the geometry path and injects them into the image path, as shown in Fig. 8. It also designs a switchable discriminator that not only classifies the RGB-D image but also regresses from the RGB image to the depth, which is compared with the depth from the generator.

Depth or normal maps work well with 2D GAN models, which can efficiently synthesize high-resolution images.

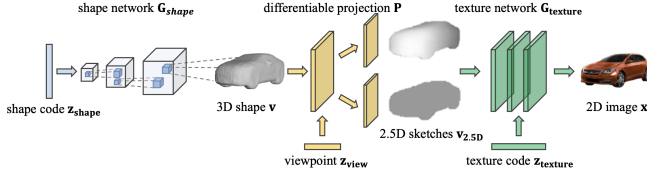


Fig. 9. VON [173] first generates the 3D shape and then render it into a depth image for image generation. Image adapted from [173].

However, 2D CNNs-based generators do not guarantee the inter-view consistency of generated images [223], even when they are supervised with the view consistency loss. Moreover, depth and normal maps are 2.5D representations that cannot show the full geometry of the scene.

5.2 Voxel Grids

There are generally two ways to synthesize images from voxel grids. The first way is using voxel grids to only represent 3D shapes, which are used to render depth maps to guide the image generation. The second way is embedding the geometry and appearance of scenes with voxel grids.

[173] and [224] are inspired from graphics rendering pipeline and decompose the image generation task into 3D shape generation and 2D image generation, which is illustrated in Fig. 9. They adopt voxel grids for the shape generation, followed by a projection operator that renders voxel grids into the depth map under a viewpoint. The depth map is further used as the guidance for RGB image generation. Similar to [182], [173] utilizes a conditional GAN to synthesize the 2D image based on the rendered depth map. To enable the illumination control, rather than directly synthesizing the appearance on the depth map, [224] generates different image components (*e.g.*, diffuse albedo, specular, and roughness) based on the rendered depth and compose the final RGB output following the physical image formation process.

[59], [67], [180] represent the underlying geometry and appearance in voxel grids simultaneously. HoloGAN [67] leverages a 3D CNN-based generator to produce a 3D feature volume from a latent vector. A projection unit will project the voxels to 2D features, and the following 2D decoder outputs the final RGB image. To control the viewpoint, HoloGAN applies 3D transformations to voxel grids, which ensures the underlying 3D geometric property. Based on HoloGAN, BlockGAN [180] generates multiple feature volumes, each representing a 3D entity, and compose them into a feature volume for the whole 3D scene. This strategy enables it to render images containing multiple objects. Instead of learning a 3D feature volume, PlatonicGAN directly [225] learns to predict RGB and alpha volumes, yet is limited to a low resolution. More recently, VoxGRAF [59] attempts to synthesize RGB and alpha volumes, and render images from volumes through the volume rendering techniques. By removing the 2D CNN renderers, VoxGRAF promises to render view-consistent images. To achieve the rendering of high-resolution images, VoxGRAF adopts sparse voxel grids to represent scenes. It first generates a low-resolution dense volume, and then

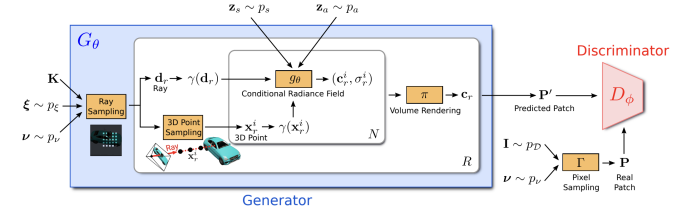


Fig. 10. GRAF [28] combines the GAN framework with neural radiance fields, which makes learning 3D image generation from single-view image collection possible. Image adapted from [28].

progressively upsamples the resolution of volume and prunes voxels in the empty space.

5.3 Neural Fields

Image synthesis methods based on neural fields generally adopt neural fields to implicitly represent the properties of each point in the 3D space, followed by a differentiable renderer to output an image under a specific viewpoint. Volume renderer [69] is the most commonly used renderer for 3D-aware image synthesis. Most of the methods use GANs to supervise the learning of neural fields.

GRAF [28] firstly introduces the concept of generative neural radiance fields. As shown in Fig. 10, a MLP-based generator is conditioned on a shape noise and an appearance noise, and predicts the density and the color of points along each ray. Then, a volume renderer gathers the information along all rays to synthesize a 2D image. Due to the slow rendering process, a patch-based discriminator is used to differentiate between the real and fake patches instead of the complete images. π -GAN [29] uses a similar setting as GRAF, but it adopts SIREN [226] rather than ReLU MLPs for representation, which is more capable of modeling fine details. It utilizes progressive training with an image-based discriminator. Besides, instead of using two latent codes, π -GAN employs a StyleGAN-like mapping network to condition the SIREN on a latent code through FiLM conditioning [227], [228]. Though improving the quality of the 3D-aware image synthesis significantly, the above methods still face with several challenges. First, the good quality of rendered images does not imply a decent underlying shape and guarantee the inter-view consistency. Second, due to the huge number of points queried along all rays and the complex rendering process, rendering an image from the model takes a lot of time. Consequently, it is hard to train a 3D-aware generative model on high-resolution images efficiently. Third, they all assume a prior distribution of camera poses on the dataset, which may not be accurate enough.

To mitigate the first issue, ShadeGAN [190] adds a lighting constraint on the generator. It generates the albedo rather than the color for each point. A shading model operates on the generated albedo map, the normal map derived from densities, the sampled camera viewpoint, and the sampled lighting source to render an RGB image. GOF [194] analyzes the weight distribution on points along a ray. The cumulative rendering process cannot ensure a low-variance distribution on rays, leading to diffused object surfaces. Occupancy-based neural fields can satisfy

the requirement but suffer from the optimization problem that gradients only exist on surfaces. Hence, GOF unifies the two representations through gradually shrinking the sampling region to a minimal neighboring region around the surface, resulting in neat surfaces and faster training. GRAM [202] also examines the point sampling strategy. It claims that deficient point sampling strategy in the prior work causes the inadequate expressiveness of the generator on fine details, and the noise caused by unstable Monte Carlo sampling leads to the inefficient GAN training. GRAM proposes to regulate the learning of neural field on 2D manifolds and only optimizes the ray-manifold intersection points. MVCGAN [205] attempts to alleviate the consistency problem by adding a multi-view constraint on the generator. For the same latent code, two camera poses are sampled for rendering and both the features and images are warped from one to the other to calculate the reprojection loss. GeoD [229] tackles the problem by making the discriminator 3D-aware. A geometry branch and a consistency branch are added to the discriminator to extract shapes and evaluate consistency from the generator’s outputs, and in turn supervise the generator.

To generate 3D-aware images on larger resolutions efficiently, a variety of methods operate neural fields in a small resolution and leverage convolutional neural networks for upsampling the image/features to a higher resolution. StyleNeRF [199] integrates the neural fields into a style-based generator. The low-resolution NeRF outputs features rather than colors which are further processed by convolutional layers. StyleSDF [201] merges a signed distance function-based representation into neural fields. The output features from the neural fields are passed to a style-based 2D generator for high-resolution generation. Two discriminators are operated on the neural field and the 2D generator separately. CIPS-3D [192] uses a shallow NeRF network to get the features and densities of all points. A deep implicit neural representation network then predicts the color of each pixel independently based on the feature vector of that pixel. Each network is accompanied by a discriminator. Despite of the high-resolution images of high fidelity achieved, introducing convolutional layers for 2D upsampling may harm the 3D consistency. Carefully designed architectures and regularizers are necessary to mitigate the problem. StyleNeRF [199] uses a well-thought-out upsampler which is based on 1x1 convolutional kernels. Moreover, a NeRF path regularizer is designed to force the output of CNNs to be similar to the output of NeRF. GRAM-HD [230] designs a super-resolution module that upsamples the manifold to a higher resolution. Images are rendered from upsampled manifolds. EpiGRAF [231] throws the convolutional neural networks away. It directly works on the output of a high-resolution neural fields through introducing a patch-based discriminator, which is modulated by the patch location and scale parameters.

Regarding camera poses, most methods assume a prior distribution from the dataset. [57], [59], [202], [230], [231], however, leverage ground-truth poses of the dataset for sampling and training. They show significantly improvement of the quality on both the images and geometry, which demonstrates the importance of an accurate camera distribution. CAMPARI [191] attempts to learn the pose

distribution from datasets automatically, and leverages a camera generator to learn the distribution shift on a prior distribution. The results show the complexity of learning poses from the dataset. Learning accurate pose distribution from a given dataset remains a difficult problem in the generation field.

With the advent of generative neural fields, researchers also explore compositional generation. GSN [232] decomposes a global neural radiance fields into several local neural radiance fields to model parts of the whole scene. GIRAFFE [30] and GIRAFFE-HD [204] represent scenes as compositional generative neural radiance fields, allowing the independent control over multiple foreground objects as well as the background.

Besides, editing and controllability in the generation process arouse the researchers’ interest. A few works focus on the semantic control in the 3D-aware generation. GANcraft [233] aims to generate realistic scene image given 3D voxel grids with semantic labels. Features of sampled points are queried through interpolation of features in voxel corners. The features are further processed by style-modulated MLPs and convolutional layers. [195] generates a semantic map from the generative radiance field conditioned on a semantic code and the sampled human pose and camera pose. It then employs an encoder-decoder structure to synthesize a human image according to the semantic map and the sampled texture latent code. The content can be manipulated through interpolating codes and sampling different poses. FENeRF [197] and IDE-3D [211] render semantic maps and color images from generative neural fields simultaneously. The semantic maps can be used to edit the 3D neural fields via GAN inversion technique [234], [235]. Pix2NeRF [236] translates a single input image to radiance field through generative models, and thus gains control in 3D space (*e.g.*, different viewpoints). An encoder is introduced before the generator to convert the input to the latent space, and forms a reconstruction objective to learn. D3D [237] decomposes the generation into two independent components of shape and appearance, enabling the control over geometry and color separately. 3D-GIF [238] and VoLux-GAN [203] seek control over lights. 3D-GIF explicitly predicts the albedo, the normal, and specular coefficients for each point in the neural field. The volume rendering and photometric image rendering are adopted to synthesize the light-aware image under a sampled lighting source. VoLux-GAN also predicts albedos, normals, diffuse components and specular components from the neural field, but uses HDR environmental map to model the lighting instead. It is hence able to do HDRI relighting.

Other than GAN-based methods, NeRF-VAE [239] leverages a variational autoencoder [16] to model the distribution of radiance fields. The model takes in a collection of images and their corresponding camera poses from the same scene as input and gets a latent variable. The latent variable is then used as the input of the generator to synthesize the content for the volume renderer. The volume renderer renders images according to the input camera poses, and the outputs are expected to be similar to the input images. LOLNeRF [240] employs auto-decoder for learning a 3D-aware generative model, where pixel-level supervision can be applied in contrast to image-pixel supervision used in

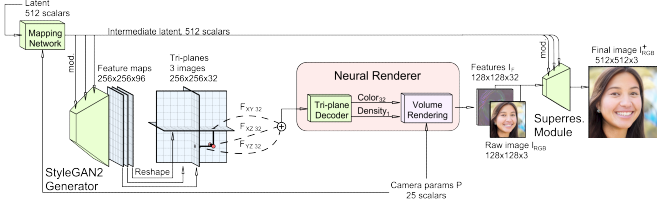


Fig. 11. EG3D [57] introduces tri-plane feature maps as the explicit representation, which efficiently encodes 3D geometry and appearance. Image adapted from [57].

GAN-based methods.

5.4 Hybrid Representations

Implicit representations can optimize the whole 3D shape well from 2D multi-view observations via differentiable rendering. So lots of works [28], [29], [30], [199], [241] choose to incorporate implicit representations into the generator to accomplish 3D-aware image synthesis. The implicit representation implemented by MLPs is memory-efficient, but evaluation takes a very long time. Explicit representations, such as voxel grids and depth, work well with CNN and are efficient for high-resolution image rendering, but they suffer from memory overhead and view consistency. The implicit and explicit representations can provide complementary benefits to each other, so combining these representations for 3D-aware image synthesis can potentially improve the image quality and rendering efficiency.

VolumeGAN [58] proposes to represent objects using structural and textural representations for 3D-aware image synthesis. To capture the structure, they first construct a feature volume and then the features queried in feature volume along with the raw coordinates, are used to learn generative implicit feature fields. A texture network akin to StyleGAN2 is used to provide texture information to the feature fields. VolumeGAN depicts 3D objects with explicit voxel grids and implicit feature fields, which improves the speed of evaluation and the quality of synthetic images. However, it is challenging to improve spatial refinement because a bigger feature volume results in a greater computing burden. Unlike VolumeGAN, EG3D [57], which is shown in Fig. 11, proposes to use tri-plane instead of voxel as the explicit representations. EG3D adopts a 2D generator to generate high-resolution tri-planes, which is easier to scale up large resolution in a computationally efficient manner. And they also adopt the similar strategy of VolumeGAN to transform the feature fields into images. Other techniques like generator pose conditioning as well as dual discrimination are also introduced to avoid view inconsistencies.

It has been shown that hybrid representations are effective in producing high-quality 3D-aware images and 3D shapes. Therefore, some following works [213], [242] also adopt tri-plane representation to achieve human synthesis. However, there is still space to improve, like training speed and strategy. For instance, VolumeGAN, relies on progressive training, which is challenging to apply when migrating to another framework.

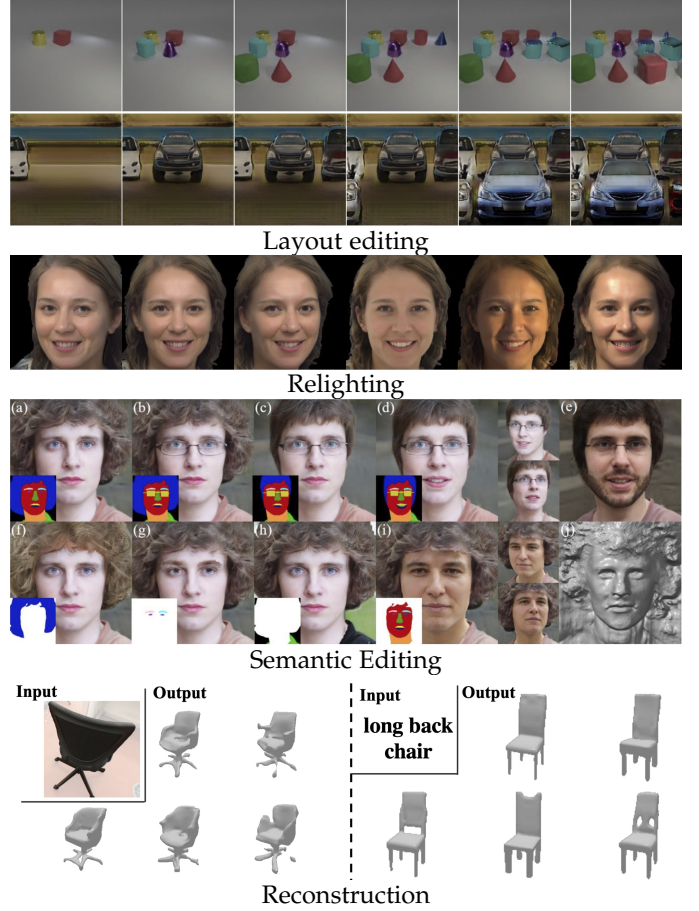


Fig. 12. 3D generative models have enabled various applications in editing, reconstruction and representation learning. Images adapted from [30] [203] [211], [60].

6 APPLICATIONS

The rise of 3D generative models has enabled many promising applications, as shown in Fig. 12. In this section, we discuss the applications of 3D generative models in terms of editing, reconstruction and representation learning.

6.1 3D Shape Editing

Many classical methods has for 3D shape editing, e.g., skeleton based deformation and cage based deformation. We refer to [243] for detailed survey of classical shape editing methods. In contrast to classical methods that directly edit the 3D shape, we focus on shape editing methods assisted by deep shape generative models.

3D space editing: Several works edit shapes relying on user manipulation in the 3D shape space. Liu et al. [244] ask users to paint 3D shapes in the form of voxel grids, assisted by a 3D GAN to refine the user-painted 3D shapes. Instead of directly editing the voxel grids, a few methods study shape editing controlled by more compact representations, including sparse 3D points or bounding boxes [135], [136], [137], [245]. While aforementioned methods focus on editing of rigid shapes, gDNA [168] enables reposing articulated human bodies controlled by human skeletons.

Latent code editing: Another set of methods updates the latent space of the generative model without user

manipulation in the 3D space. Part-aware generative models naturally comes with part-level controllability [125], [166]. Several methods explore shape editing guided by semantic labels or language descriptions [246], [247], [248].

6.2 3D-Aware Image Editing

As 3D-aware image generative models introduces physically meaningful 3D factors to the image formation process, the editing of 3D-aware image generative models can be categorized into two categories. One line of works edits the physically meaningful 3D factors, and the other manipulates the latent code.

Physical factor editing: All 3D-aware image synthesis methods allow users to control camera poses, resulting in 2D images of various viewpoints [28], [29], [57], [199], [201], [202]. In addition to camera poses, several methods [30], [180], [249] enable editing of object poses, inserting new objects by modeling the compositional nature of the scene. Re-lighting is also studied via disentangling the albedo, normal, and specular coefficients [194], [203], [238]. More recently, several generative models for neural articulated radiance fields are proposed for human bodies [206], [213], [242], enabling shape manipulation driven by human skeletons.

Latent code editing: The latent code models all the other variations that are not captured by the physically meaningful 3D factors, e.g., object shape and appearance. One line of works allows for editing the global attributes of the generated contents. Several methods learn disentangled shape and appearance code for generative radiance fields, enabling independent interpolation of shape and appearance [28], [237]. CLIP-NeRF [250] further allows for controlling shape and appearance of generative radiance fields using language or a guidance image. Another line of works explores more fine-grained, local editing. FENeRF [197] and IDE-3D [211] enables semantic editing of generative radiance fields guided by semantic segmentation masks.

6.3 3D Shape Reconstruction

There are two common choices for leveraging 3D generative models for reconstruction, depending on whether test-time optimization is applied for reconstruction or not.

Armotized inference: Generative models equipped with an encoder (e.g., VAE) naturally enables reconstructing 3D shapes from a given input. In contrast to standard 3D reconstruction that focus on one-to-one mapping from the input to the target 3D shape, generative methods allows for sampling many possible shapes from the posterior distribution. This line of works is applicable to different types of input by switching the encoder. The common choices of input include single-view image [60], [251], point cloud [251], low-resolution voxel grid, and text description. **Model inversion:** Another line of methods leverages the inversion of generative models for reconstruction, typically requiring test-time optimization. Adopting an auto-decoder framework, a complete shape can be reconstructed from a partial observation via optimizing the latent code to match the partial observation [143], [252].

While aforementioned methods only allow for reconstructing shapes based on 3D shape generative models,

more recent works demonstrate single-view image based 3D reconstruction by inverting the 3D-aware image generative models [29], [57]. This line of works follows a classical idea of Analysis by Synthesis [253]. Note that by inverting 3D-aware generative models, camera poses can also be recovered, thus enabling category-level object pose estimation [254], [255].

6.4 Representation Learning

Another common application of generative models is to learn better representations for downstream tasks, e.g., classification or segmentation. Representation learning on point clouds has been demonstrated to be effective for model classification and semantic segmentation [26], [128], [256]. Generative models of voxel grids are also adopted for model classification, shape recovery and super-resolution [107].

7 FUTURE WORK

The development of 3D generative models has advanced rapidly, but there are still a lot of challenges to overcome before they can be used for downstream applications, such as gaming, simulation, and augmented/virtual reality. Here, we discuss promising future directions of 3D generative models.

Universality: Most of existing 3D generative models are trained on simple object-level datasets, e.g., ShapeNet for 3D shape generation and FFHQ for 3D-aware image synthesis. We believe that the extension of 3D generative models to a greater degree of universality is a fruitful direction for future research. The universality includes generating versatile objects (e.g., ImageNet or Microsoft CoCo), dynamic objects or scenes, and large-scale scenes. Instead of focusing on a single category, it is of particular interesting to learn a general 3D generative model for various categories like DALL-E2 and Imagen [257], [258] and infinite 3D scenes [259].

Controllability: The controllability of 3D generative models lags behind that of 2D generative models. Ideally, the user should be able to control the 3D generation process via user-friendly input, including but not limited to language, sketch and program. Moreover, we believe that the controllability over the physical properties should be further investigated, including lighting, material and even dynamics.

Efficiency: Many 3D generative models require 3-10 days of training on multiple high-end GPUs and are slow during inference. We believe that improving the training efficiency 3D generative models is desired, and enhancing the inference efficiency is crucial for downstream applications.

Training stability: The training of 3D generative models, in particular 3D-aware image synthesis models, is usually more prone to mode collapse. One possible explanation is that the distribution of the physically meaningful factors, e.g., camera poses and rendering parameters, may not match that of the real images. Investigating the training stability of generative models is thus particularly important.

8 CONCLUSION

Deep 3D generative models, such as VAEs and GANs, aim to characterize the data distribution of observed 3D data.

A key challenge in the task of 3D generation is that there are many 3D representations for describing 3D instances and each representation exhibits its own advantage and disadvantage in generative modeling. This paper presents a comprehensive review of 3D generation by discussing how different 3D representations work with different generative models. We first introduce fundamentals of 3D generative models, including the formulation of generative models and 3D representations. Then, we review how 3D representations are modeled and generated in the task of 3D shape generation and 3D-aware image generation, respectively. The applications of 3D generative models are then discussed, including shape editing, 3D-aware image manipulation, reconstruction, and representation learning. Finally, we discuss the limitations of existing 3D generative models and propose some future directions of 3D generation. We hope this review can help the readers grasp a better understanding of the 3D generation field and inspire more works in the future.

REFERENCES

- [1] Y. LeCun, Y. Bengio, and G. Hinton, "Deep learning," *Nature*, 2015. **1**
- [2] A. Krizhevsky, I. Sutskever, and G. E. Hinton, "Imagenet classification with deep convolutional neural networks," in *NeurIPS*, 2012. **1**
- [3] K. Simonyan and A. Zisserman, "Very deep convolutional networks for large-scale image recognition," *arXiv preprint arXiv:1409.1556*, 2014. **1**
- [4] R. Girshick, "Fast r-cnn," in *ICCV*, 2015. **1**
- [5] S. Ren, K. He, R. Girshick, and J. Sun, "Faster r-cnn: Towards real-time object detection with region proposal networks," *NeurIPS*, 2015. **1**
- [6] K. He, G. Gkioxari, P. Dollár, and R. Girshick, "Mask r-cnn," in *ICCV*, 2017. **1**
- [7] M. Oechsle, S. Peng, and A. Geiger, "Unisurf: Unifying neural implicit surfaces and radiance fields for multi-view reconstruction," in *ICCV*, 2021. **1, 5**
- [8] L. Yariv, J. Gu, Y. Kasten, and Y. Lipman, "Volume rendering of neural implicit surfaces," *NeurIPS*, 2021. **1, 5**
- [9] B. Mildenhall, P. P. Srinivasan, M. Tancik, J. T. Barron, R. Ramamoorthi, and R. Ng, "Nerf: Representing scenes as neural radiance fields for view synthesis," in *ECCV*, 2020. **1, 5**
- [10] D. Xu, D. Anguelov, and A. Jain, "Pointfusion: Deep sensor fusion for 3d bounding box estimation," in *CVPR*, 2018. **1**
- [11] M.-F. Chang, J. Lambert, P. Sangkloy, J. Singh, S. Bak, A. Hartnett, D. Wang, P. Carr, S. Lucey, D. Ramanan *et al.*, "Argoverse: 3d tracking and forecasting with rich maps," in *CVPR*, 2019. **1**
- [12] J. Jumper, R. Evans, A. Pritzel, T. Green, M. Figurnov, O. Ronneberger, K. Tunyasuvunakool, R. Bates, A. Židek, A. Potapenko *et al.*, "Highly accurate protein structure prediction with alphafold," *Nature*, 2021. **1**
- [13] A. Ramesh, M. Pavlov, G. Goh, S. Gray, C. Voss, A. Radford, M. Chen, and I. Sutskever, "Zero-shot text-to-image generation," in *ICML*, 2021. **1**
- [14] A. Ramesh, P. Dhariwal, A. Nichol, C. Chu, and M. Chen, "Hierarchical text-conditional image generation with clip latents," *arXiv preprint arXiv:2204.06125*, 2022. **1**
- [15] I. Goodfellow, J. Pouget-Abadie, M. Mirza, B. Xu, D. Warde-Farley, S. Ozair, A. Courville, and Y. Bengio, "Generative adversarial nets," in *NeurIPS*, 2014. **1, 2**
- [16] D. P. Kingma and M. Welling, "Auto-encoding variational bayes," in *ICLR*, 2014. **1, 2, 3, 13**
- [17] J. Ho, A. Jain, and P. Abbeel, "Denoising diffusion probabilistic models," *NeurIPS*, 2020. **1, 2, 3**
- [18] Y. Xu, Y. Shen, J. Zhu, C. Yang, and B. Zhou, "Generative hierarchical features from synthesizing images," in *CVPR*, 2021. **1**
- [19] P. Isola, J.-Y. Zhu, T. Zhou, and A. A. Efros, "Image-to-image translation with conditional adversarial networks," in *CVPR*, 2017. **1**
- [20] Y. Shen, C. Yang, X. Tang, and B. Zhou, "Interfacegan: Interpreting the disentangled face representation learned by gans," *TPAMI*, 2020. **1**
- [21] C. Saharia, W. Chan, S. Saxena, L. Li, J. Whang, E. Denton, S. K. S. Ghasemipour, B. K. Ayan, S. S. Mahdavi, R. G. Lopes *et al.*, "Photorealistic text-to-image diffusion models with deep language understanding," *arXiv preprint arXiv:2205.11487*, 2022. **1**
- [22] J. Yu, Y. Xu, J. Y. Koh, T. Luong, G. Baid, Z. Wang, V. Vasudevan, A. Ku, Y. Yang, B. K. Ayan *et al.*, "Scaling autoregressive models for content-rich text-to-image generation," *arXiv preprint arXiv:2206.10789*, 2022. **1**
- [23] Y. Bengio, R. Ducharme, and P. Vincent, "A neural probabilistic language model," *NeurIPS*, 2000. **1**
- [24] D. Rezende and S. Mohamed, "Variational inference with normalizing flows," in *ICML*, 2015. **1, 2**
- [25] J. Wu, C. Zhang, T. Xue, B. Freeman, and J. Tenenbaum, "Learning a probabilistic latent space of object shapes via 3d generative-adversarial modeling," in *NeurIPS*, 2016. **1, 6, 7**
- [26] P. Achlioptas, O. Diamanti, I. Mitliagkas, and L. Guibas, "Learning representations and generative models for 3d point clouds," in *ICML*, 2018. **1, 6, 8, 10, 15**
- [27] Z. Chen and H. Zhang, "Learning implicit fields for generative shape modeling," in *CVPR*, 2019. **1, 6, 9**
- [28] K. Schwarz, Y. Liao, M. Niemeyer, and A. Geiger, "Graf: Generative radiance fields for 3d-aware image synthesis," *NeurIPS*, 2020. **1, 11, 12, 14, 15**
- [29] E. R. Chan, M. Monteiro, P. Kellnhofer, J. Wu, and G. Wetzstein, "pi-gan: Periodic implicit generative adversarial networks for 3d-aware image synthesis," in *CVPR*, 2021. **1, 11, 12, 14, 15**
- [30] M. Niemeyer and A. Geiger, "Giraffe: Representing scenes as compositional generative neural feature fields," in *CVPR*, 2021. **1, 11, 13, 14, 15**
- [31] C. R. Qi, H. Su, K. Mo, and L. J. Guibas, "Pointnet: Deep learning on point sets for 3d classification and segmentation," in *CVPR*, 2017. **1, 4, 8, 10**
- [32] C. R. Qi, L. Yi, H. Su, and L. J. Guibas, "Pointnet++: Deep hierarchical feature learning on point sets in a metric space," *NeurIPS*, 2017. **1, 4**
- [33] A. Sinha, A. Unmesh, Q. Huang, and K. Ramani, "Surfnet: Generating 3d shape surfaces using deep residual networks," in *CVPR*, 2017. **1, 5**
- [34] N. Wang, Y. Zhang, Z. Li, Y. Fu, W. Liu, and Y.-G. Jiang, "Pixel2mesh: Generating 3d mesh models from single rgb images," in *ECCV*, 2018. **1, 5**
- [35] Z. Wu, S. Song, A. Khosla, F. Yu, L. Zhang, X. Tang, and J. Xiao, "3d shapenets: A deep representation for volumetric shapes," in *CVPR*, 2015. **1, 4, 6, 7**
- [36] D. Maturana and S. Scherer, "Voxnet: A 3d convolutional neural network for real-time object recognition," in *IROS*, 2015. **1, 4, 7**
- [37] T. Zhou, R. Tucker, J. Flynn, G. Fyfe, and N. Snavely, "Stereo magnification: Learning view synthesis using multiplane images," in *SIGGRAPH*, 2018. **1, 4**
- [38] A. Oussidi and A. Elhassouny, "Deep generative models: Survey," in *ISCV*, 2018. **2**
- [39] S. Bond-Taylor, A. Leach, Y. Long, and C. G. Willcocks, "Deep generative modelling: A comparative review of vases, gans, normalizing flows, energy-based and autoregressive models," *arXiv preprint arXiv:2103.04922*, 2021. **2**
- [40] A. Tewari, J. Thies, B. Mildenhall, P. Srinivasan, E. Tretschk, W. Yifan, C. Lassner, V. Sitzmann, R. Martin-Brualla, S. Lombardi *et al.*, "Advances in neural rendering," in *CGF*, 2022. **2**
- [41] Y. Guo, H. Wang, Q. Hu, H. Liu, L. Liu, and M. Bennamoun, "Deep learning for 3d point clouds: A survey," *TPAMI*, 2020. **2**
- [42] J. Lahoud, J. Cao, F. S. Khan, H. Cholakkal, R. M. Anwer, S. Khan, and M.-H. Yang, "3d vision with transformers: A survey," *arXiv preprint arXiv:2208.04309*, 2022. **2**
- [43] Y. Xie, T. Takikawa, S. Saito, O. Litany, S. Yan, N. Khan, F. Tombari, J. Tompkin, V. Sitzmann, and S. Sridhar, "Neural fields in visual computing and beyond," in *CGF*, 2022. **2, 4**
- [44] S. Chaudhuri, D. Ritchie, J. Wu, K. Xu, and H. Zhang, "Learning generative models of 3d structures," in *CGF*, 2020. **2**
- [45] M. Toshpulatov, W. Lee, and S. Lee, "Generative adversarial networks and their application to 3d face generation: A survey," *Image and Vision Computing*, 2021. **2**

- [46] M. Zollhöfer, P. Stotko, A. Görlitz, C. Theobalt, M. Nießner, R. Klein, and A. Kolb, "State of the art on 3d reconstruction with rgb-d cameras," in *CGF*, 2018. 2
- [47] H. Kato, D. Beker, M. Morariu, T. Ando, T. Matsuoka, W. Kehl, and A. Gaidon, "Differentiable rendering: A survey," *arXiv preprint arXiv:2006.12057*, 2020. 2
- [48] G. E. Hinton, "Training products of experts by minimizing contrastive divergence," *Neural computation*, 2002. 2
- [49] A. Radford, L. Metz, and S. Chintala, "Unsupervised representation learning with deep convolutional generative adversarial networks," in *ICLR*, 2016. 2
- [50] T. Karras, T. Aila, S. Laine, and J. Lehtinen, "Progressive growing of gans for improved quality, stability, and variation," in *ICLR*, 2018. 2, 11
- [51] T. Karras, S. Laine, and T. Aila, "A style-based generator architecture for generative adversarial networks," in *CVPR*, 2019. 2, 11
- [52] T. Karras, S. Laine, M. Aittala, J. Hellsten, J. Lehtinen, and T. Aila, "Analyzing and improving the image quality of StyleGAN," in *CVPR*, 2020. 2
- [53] T. Karras, M. Aittala, S. Laine, E. Härkönen, J. Hellsten, J. Lehtinen, and T. Aila, "Alias-free generative adversarial networks," in *NeurIPS*, 2021. 2
- [54] D. M. Blei, A. Kucukelbir, and J. D. McAuliffe, "Variational inference: A review for statisticians," *J. of the American statist. Associat.*, 2017. 3
- [55] N. Karmakar, A. Biswas, P. Bhowmick, and B. B. Bhattacharya, "A combinatorial algorithm to construct 3d isothetic covers," *International Journal of Computer Mathematics*, 2013. 4
- [56] J. Yang, X. Lu, and W. Chen, "A robust scheme for 3d point cloud copy detection," *arXiv preprint arXiv:2110.00972*, 2021. 4
- [57] E. R. Chan, C. Z. Lin, M. A. Chan, K. Nagano, B. Pan, S. De Mello, O. Gallo, L. J. Guibas, J. Tremblay, S. Khamis *et al.*, "Efficient geometry-aware 3d generative adversarial networks," in *CVPR*, 2022. 4, 6, 11, 13, 14, 15
- [58] Y. Xu, S. Peng, C. Yang, Y. Shen, and B. Zhou, "3d-aware image synthesis via learning structural and textural representations," in *CVPR*, 2022. 4, 11, 14
- [59] K. Schwarz, A. Sauer, M. Niemeyer, Y. Liao, and A. Geiger, "Voxgraf: Fast 3d-aware image synthesis with sparse voxel grids," in *NeurIPS*, 2022. 4, 12, 13
- [60] P. Mittal, Y.-C. Cheng, M. Singh, and S. Tulsiani, "Autosdf: Shape priors for 3d completion, reconstruction and generation," in *CVPR*, 2022. 4, 6, 7, 14, 15
- [61] C. B. Choy, D. Xu, J. Gwak, K. Chen, and S. Savarese, "3d-r2n2: A unified approach for single and multi-view 3d object reconstruction," in *ECCV*, 2016. 4
- [62] C. Häne, S. Tulsiani, and J. Malik, "Hierarchical surface prediction for 3d object reconstruction," in *3DV*, 2017. 4
- [63] M. Tatarchenko, A. Dosovitskiy, and T. Brox, "Octree generating networks: Efficient convolutional architectures for high-resolution 3d outputs," in *ICCV*, 2017. 4
- [64] G. Riegler, A. Osman Ulusoy, and A. Geiger, "Octnet: Learning deep 3d representations at high resolutions," in *CVPR*, 2017. 4
- [65] P.-S. Wang, Y. Liu, Y.-X. Guo, C.-Y. Sun, and X. Tong, "Ocnn: Octree-based convolutional neural networks for 3d shape analysis," *TOG*, 2017. 4
- [66] V. Sitzmann, J. Thies, F. Heide, M. Nießner, G. Wetzstein, and M. Zollhofer, "Deepvoxels: Learning persistent 3d feature embeddings," in *CVPR*, 2019. 4
- [67] T. Nguyen-Phuoc, C. Li, L. Theis, C. Richardt, and Y.-L. Yang, "Hologan: Unsupervised learning of 3d representations from natural images," in *ICCV*, 2019. 4, 11, 12
- [68] S. Lombardi, T. Simon, J. Saragih, G. Schwartz, A. Lehrmann, and Y. Sheikh, "Neural volumes: Learning dynamic renderable volumes from images," *TOG*, 2019. 4
- [69] J. T. Kajiya and B. P. Von Herzen, "Ray tracing volume densities," *SIGGRAPH*, 1984. 4, 5, 12
- [70] H. Fan, H. Su, and L. J. Guibas, "A point set generation network for 3d object reconstruction from a single image," in *CVPR*, 2017. 4
- [71] Y. Li, R. Bu, M. Sun, W. Wu, X. Di, and B. Chen, "Pointcnn: Convolution on x-transformed points," *NeurIPS*, 2018. 4
- [72] Y. Wang, Y. Sun, Z. Liu, S. E. Sarma, M. M. Bronstein, and J. M. Solomon, "Dynamic graph cnn for learning on point clouds," *TOG*, 2019. 4
- [73] S. Shi, C. Guo, L. Jiang, Z. Wang, J. Shi, X. Wang, and H. Li, "Pv-rcnn: Point-voxel feature set abstraction for 3d object detection," in *CVPR*, 2020. 4
- [74] M. Meshry, D. B. Goldman, S. Khamis, H. Hoppe, R. Pandey, N. Snavely, and R. Martin-Brualla, "Neural rerendering in the wild," in *CVPR*, 2019. 4
- [75] W. Yifan, F. Serena, S. Wu, C. Öztireli, and O. Sorkine-Hornung, "Differentiable surface splatting for point-based geometry processing," *TOG*, 2019. 4
- [76] C. Lassner and M. Zollhofer, "Pulsar: Efficient sphere-based neural rendering," in *CVPR*, 2021. 4
- [77] M. Wu, Y. Wang, Q. Hu, and J. Yu, "Multi-view neural human rendering," in *CVPR*, 2020. 5
- [78] K.-A. Aliev, A. Sevastopolsky, M. Kolos, D. Ulyanov, and V. Lempitsky, "Neural point-based graphics," in *ECCV*, 2020. 5
- [79] O. Wiles, G. Gkioxari, R. Szeliski, and J. Johnson, "SynSin: End-to-end view synthesis from a single image," in *CVPR*, 2020. 5
- [80] D. Rückert, L. Franke, and M. Stamminger, "Adop: Approximate differentiable one-pixel point rendering," *TOG*, 2022. 5
- [81] Q. Xu, Z. Xu, J. Philip, S. Bi, Z. Shu, K. Sunkavalli, and U. Neumann, "Point-nerf: Point-based neural radiance fields," in *CVPR*, 2022. 5
- [82] D. Zimny, T. Trzciński, and P. Spurek, "Points2nerf: Generating neural radiance fields from 3d point cloud," *arXiv preprint arXiv:2206.01290*, 2022. 5, 6
- [83] J. Huang, H. Zhang, L. Yi, T. Funkhouser, M. Nießner, and L. J. Guibas, "Texturenet: Consistent local parametrizations for learning from high-resolution signals on meshes," in *CVPR*, 2019. 5
- [84] N. Verma, E. Boyer, and J. Verbeek, "Featnet: Feature-steered graph convolutions for 3d shape analysis," in *CVPR*, 2018. 5
- [85] R. Hanocka, A. Hertz, N. Fish, R. Giryes, S. Fleishman, and D. Cohen-Or, "Meshcnn: a network with an edge," *TOG*, 2019. 5
- [86] Y. Zhou, C. Wu, Z. Li, C. Cao, Y. Ye, J. Saragih, H. Li, and Y. Sheikh, "Fully convolutional mesh autoencoder using efficient spatially varying kernels," *NeurIPS*, 2020. 5
- [87] M. Fey, J. E. Lenssen, F. Weichert, and H. Müller, "Splinecnn: Fast geometric deep learning with continuous b-spline kernels," in *CVPR*, 2018. 5
- [88] C. Wen, Y. Zhang, Z. Li, and Y. Fu, "Pixel2mesh++: Multi-view 3d mesh generation via deformation," in *ICCV*, 2019. 5
- [89] S. Goel, A. Kanazawa, and J. Malik, "Shape and viewpoint without keypoints," in *ECCV*, 2020. 5
- [90] A. Kanazawa, S. Tulsiani, A. A. Efros, and J. Malik, "Learning category-specific mesh reconstruction from image collections," in *ECCV*, 2018. 5
- [91] J. Pan, X. Han, W. Chen, J. Tang, and K. Jia, "Deep mesh reconstruction from single rgb images via topology modification networks," in *ICCV*, 2019. 5
- [92] M. M. Loper and M. J. Black, "Opendr: An approximate differentiable renderer," in *ECCV*, 2014. 5
- [93] H. Kato, Y. Ushiku, and T. Harada, "Neural 3d mesh renderer," in *CVPR*, 2018. 5
- [94] S. Liu, T. Li, W. Chen, and H. Li, "Soft rasterizer: A differentiable renderer for image-based 3d reasoning," in *ICCV*, 2019. 5
- [95] J. Thies, M. Zollhöfer, and M. Nießner, "Deferred neural rendering: Image synthesis using neural textures," *TOG*, 2019. 5
- [96] A. Raj, J. Tanke, J. Hays, M. Vo, C. Stoll, and C. Lassner, "Anr: Articulated neural rendering for virtual avatars," in *CVPR*, 2021. 5
- [97] J. Gao, W. Chen, T. Xiang, A. Jacobson, M. McGuire, and S. Fidler, "Learning deformable tetrahedral meshes for 3d reconstruction," *NeurIPS*, 2020. 5, 6
- [98] B. Yang, C. Bao, J. Zeng, H. Bao, Y. Zhang, Z. Cui, and G. Zhang, "Neumesh: Learning disentangled neural mesh-based implicit field for geometry and texture editing," in *ECCV*, 2022. 5, 6
- [99] A. Paszke, S. Gross, F. Massa, A. Lerer, J. Bradbury, G. Chanan, T. Killeen, Z. Lin, N. Gimelshein, L. Antiga, A. Desmaison, A. Kopf, E. Yang, Z. DeVito, M. Raison, A. Tejani, S. Chilamkurthy, B. Steiner, L. Fang, J. Bai, and S. Chintala, "Pytorch: An imperative style, high-performance deep learning library," in *NeurIPS*, 2019. 6
- [100] J. J. Lim, H. Pirsiavash, and A. Torralba, "Parsing ikea objects: Fine pose estimation," in *ICCV*, 2013. 6

- [101] A. Brock, T. Lim, J. M. Ritchie, and N. Weston, "Generative and discriminative voxel modeling with convolutional neural networks," *arXiv preprint arXiv:1608.04236*, 2016. 6, 7
- [102] Z. Wu, X. Wang, D. Lin, D. Lischinski, D. Cohen-Or, and H. Huang, "Sagnet: Structure-aware generative network for 3d-shape modeling," *TOG*, 2019. 6, 7
- [103] Y. Guan, T. Jahan, and O. van Kaick, "Generalized autoencoder for volumetric shape generation," in *CVPRW*, 2020. 6
- [104] Y. Wang, S. Asafi, O. van Kaick, H. Zhang, D. Cohen-Or, and B. Chen, "Active co-analysis of a set of shapes," *TOG*, 2012. 6
- [105] R. Wu, Y. Zhuang, K. Xu, H. Zhang, and B. Chen, "Pq-net: A generative part seq2seq network for 3d shapes," in *CVPR*, 2020. 6, 7
- [106] K. Mo, S. Zhu, A. X. Chang, L. Yi, S. Tripathi, L. J. Guibas, and H. Su, "Partnet: A large-scale benchmark for fine-grained and hierarchical part-level 3d object understanding," in *CVPR*, 2019. 6
- [107] J. Xie, Z. Zheng, R. Gao, W. Wang, S.-C. Zhu, and Y. N. Wu, "Generative voxelnet: learning energy-based models for 3d shape synthesis and analysis," *TPAMI*, 2020. 6, 15
- [108] A. X. Chang, T. Funkhouser, L. Guibas, P. Hanrahan, Q. Huang, Z. Li, S. Savarese, M. Savva, S. Song, H. Su *et al.*, "Shapenet: An information-rich 3d model repository," *arXiv preprint arXiv:1512.03012*, 2015. 6, 7, 11
- [109] F. Bogo, J. Romero, G. Pons-Moll, and M. J. Black, "Dynamic FAUST: Registering human bodies in motion," in *CVPR*, 2017. 6
- [110] M. Gadelha, R. Wang, and S. Maji, "Multiresolution tree networks for 3d point cloud processing," in *ECCV*, 2018. 6
- [111] D. W. Shu, S. W. Park, and J. Kwon, "3d point cloud generative adversarial network based on tree structured graph convolutions," in *ICCV*, 2019. 6, 8
- [112] C.-L. Li, M. Zaheer, Y. Zhang, B. Póczos, and R. Salakhutdinov, "Point cloud gan," *arXiv preprint arXiv:1810.05795*, 2018. 6, 8
- [113] D. Valsesia, G. Fracastoro, and E. Magli, "Learning localized generative models for 3d point clouds via graph convolution," in *ICLR*, 2018. 6, 8
- [114] G. Yang, X. Huang, Z. Hao, M.-Y. Liu, S. Belongie, and B. Hariharan, "Pointflow: 3d point cloud generation with continuous normalizing flows," in *ICCV*, 2019. 6, 8
- [115] S. Ramasinghe, S. Khan, N. Barnes, and S. Gould, "Spectral-gans for high-resolution 3d point-cloud generation," in *IROS*, 2020. 6, 8
- [116] L. Hui, R. Xu, J. Xie, J. Qian, and J. Yang, "Progressive point cloud deconvolution generation network," in *ECCV*, 2020. 6, 8
- [117] M. S. Arshad and W. J. Beks, "A progressive conditional generative adversarial network for generating dense and colored 3d point clouds," in *3DV*, 2020. 6, 8
- [118] M. Zamorski, M. Zieba, P. Klukowski, R. Nowak, K. Kurach, W. Stokowiec, and T. Trzciński, "Adversarial autoencoders for compact representations of 3d point clouds," *CVIU*, 2020. 6, 8
- [119] R. Cai, G. Yang, H. Averbuch-Elor, Z. Hao, S. Belongie, N. Snavely, and B. Hariharan, "Learning gradient fields for shape generation," in *ECCV*, 2020. 6, 9
- [120] W. Yifan, S. Wu, H. Huang, D. Cohen-Or, and O. Sorkine-Hornung, "Patch-based progressive 3d point set upsampling," in *CVPR*, 2019. 6
- [121] H. Kim, H. Lee, W. H. Kang, J. Y. Lee, and N. S. Kim, "Softflow: Probabilistic framework for normalizing flow on manifolds," in *NeurIPS*, 2020. 6, 9
- [122] R. Klokov, E. Boyer, and J. Verbeek, "Discrete point flow networks for efficient point cloud generation," in *ECCV*, 2020. 6, 9
- [123] Y. Sun, Y. Wang, Z. Liu, J. Siegel, and S. Sarma, "Pointgrow: Autoregressively learned point cloud generation with self-attention," in *WACV*, 2020. 6, 9, 10
- [124] Y. Xiang, R. Mottaghi, and S. Savarese, "Beyond pascal: A benchmark for 3d object detection in the wild," in *WACV*, 2014. 6
- [125] R. Li, X. Li, K.-H. Hui, and C.-W. Fu, "Sp-gan: Sphere-guided 3d shape generation and manipulation," *TOG*, 2021. 6, 9, 15
- [126] M. Loper, N. Mahmood, J. Romero, G. Pons-Moll, and M. J. Black, "SMPL: A skinned multi-person linear model," *TOG*, 2015. 6
- [127] S. Zuffi, A. Kanazawa, D. Jacobs, and M. J. Black, "3D menagerie: Modeling the 3D shape and pose of animals," in *CVPR*, 2017. 6
- [128] J. Xie, Y. Xu, Z. Zheng, S.-C. Zhu, and Y. N. Wu, "Generative pointnet: Deep energy-based learning on unordered point sets for 3d generation, reconstruction and classification," in *CVPR*, 2021. 6, 9, 15
- [129] S. Luo and W. Hu, "Diffusion probabilistic models for 3d point cloud generation," in *CVPR*, 2021. 6, 9
- [130] C. Nash, Y. Ganin, S. A. Eslami, and P. Battaglia, "Polygen: An autoregressive generative model of 3d meshes," in *ICML*, 2020. 6, 10
- [131] L. Gao, T. Wu, Y.-J. Yuan, M.-X. Lin, Y.-K. Lai, and H. Zhang, "Tm-net: Deep generative networks for textured meshes," *TOG*, 2021. 6, 10
- [132] H. Ben-Hamu, H. Maron, I. Kezurer, G. Avineri, and Y. Lipman, "Multi-chart generative surface modeling," *TOG*, 2018. 6, 10
- [133] L. Pishchulin, S. Wuhler, T. Helten, C. Theobalt, and B. Schiele, "Building statistical shape spaces for 3d human modeling," *PR*, 2017. 6
- [134] M. Kleineberg, M. Fey, and F. Weichert, "Adversarial generation of continuous implicit shape representations," *arXiv preprint arXiv:2002.00349*, 2020. 6, 10
- [135] Z. Hao, H. Averbuch-Elor, N. Snavely, and S. Belongie, "Dualsdf: Semantic shape manipulation using a two-level representation," in *CVPR*, 2020. 6, 9, 14
- [136] M. Ibing, I. Lim, and L. Kobbelt, "3d shape generation with grid-based implicit functions," in *CVPR*, 2021. 6, 10, 14
- [137] Y. Deng, J. Yang, and X. Tong, "Deformed implicit field: Modeling 3d shapes with learned dense correspondence," in *CVPR*, 2021. 6, 9, 14
- [138] L. Yi, V. G. Kim, D. Ceylan, I.-C. Shen, M. Yan, H. Su, C. Lu, Q. Huang, A. Sheffer, and L. Guibas, "A scalable active framework for region annotation in 3d shape collections," *TOG*, 2016. 6
- [139] X. Chen, T. Jiang, J. Song, J. Yang, M. J. Black, A. Geiger, and O. Hilliges, "gdna: Towards generative detailed neural avatars," in *CVPR*, 2022. 6
- [140] G. Tiwari, B. L. Bhatnagar, T. Tung, and G. Pons-Moll, "Sizer: A dataset and model for parsing 3d clothing and learning size sensitive 3d clothing," in *ECCV*, 2020. 6
- [141] R. K. Jones, T. Barton, X. Xu, K. Wang, E. Jiang, P. Guerrero, N. J. Mitra, and D. Ritchie, "Shapeassembly: Learning to generate programs for 3d shape structure synthesis," *TOG*, 2020. 6, 10
- [142] L. Mescheder, M. Oechsle, M. Niemeyer, S. Nowozin, and A. Geiger, "Occupancy networks: Learning 3d reconstruction in function space," in *CVPR*, 2019. 5
- [143] J. J. Park, P. Florence, J. Straub, R. Newcombe, and S. Lovegrove, "DeepSDF: Learning continuous signed distance functions for shape representation," in *CVPR*, 2019. 5, 15
- [144] P. Wang, L. Liu, Y. Liu, C. Theobalt, T. Komura, and W. Wang, "Neus: Learning neural implicit surfaces by volume rendering for multi-view reconstruction," *NeurIPS*, 2021. 5
- [145] M. Niemeyer, L. Mescheder, M. Oechsle, and A. Geiger, "Differentiable volumetric rendering: Learning implicit 3d representations without 3d supervision," in *CVPR*, 2020. 5
- [146] J. C. Hart, "Sphere tracing: A geometric method for the antialiased ray tracing of implicit surfaces," *The Visual Computer*, 1996. 5
- [147] T. Takikawa, J. Litalien, K. Yin, K. Kreis, C. Loop, D. Nowrouzezahrai, A. Jacobson, M. McGuire, and S. Fidler, "Neural geometric level of detail: Real-time rendering with implicit 3d shapes," in *CVPR*, 2021. 5
- [148] L. Liu, J. Gu, K. Zaw Lin, T.-S. Chua, and C. Theobalt, "Neural sparse voxel fields," *NeurIPS*, 2020. 5, 6
- [149] D. B. Lindell, J. N. Martel, and G. Wetzstein, "Autoint: Automatic integration for fast neural volume rendering," in *CVPR*, 2021. 5
- [150] A. Yu, R. Li, M. Tancik, H. Li, R. Ng, and A. Kanazawa, "Plenotrees for real-time rendering of neural radiance fields," in *ICCV*, 2021. 5
- [151] P. Hedman, P. P. Srinivasan, B. Mildenhall, J. T. Barron, and P. Debevec, "Baking neural radiance fields for real-time view synthesis," in *ICCV*, 2021. 5, 6
- [152] S. J. Garbin, M. Kowalski, M. Johnson, J. Shotton, and J. Valentin, "Fastnerf: High-fidelity neural rendering at 200fps," in *ICCV*, 2021. 5
- [153] C. Reiser, S. Peng, Y. Liao, and A. Geiger, "Kilonerf: Speeding up neural radiance fields with thousands of tiny mlps," in *ICCV*, 2021. 5
- [154] S. Fridovich-Keil, A. Yu, M. Tancik, Q. Chen, B. Recht, and A. Kanazawa, "Plenoxels: Radiance fields without neural networks," in *CVPR*, 2022. 6

- [155] J. Li, Z. Feng, Q. She, H. Ding, C. Wang, and G. H. Lee, "Mine: Towards continuous depth mpi with nerf for novel view synthesis," in *ICCV*, 2021. 6
- [156] Q. Xu, Z. Xu, J. Philip, S. Bi, Z. Shu, K. Sunkavalli, and U. Neumann, "Point-nerf: Point-based neural radiance fields," in *CVPR*, 2022. 6
- [157] Y. Zhou and O. Tuzel, "Voxelnet: End-to-end learning for point cloud based 3d object detection," in *CVPR*, 2018. 7
- [158] J. Mao, Y. Xue, M. Niu, H. Bai, J. Feng, X. Liang, H. Xu, and C. Xu, "Voxel transformer for 3d object detection," in *ICCV*, 2021. 7
- [159] M. Zhao, Q. Liu, A. Jha, R. Deng, T. Yao, A. Mahadevan-Jansen, M. J. Tyska, B. A. Millis, and Y. Huo, "Voxelembd: 3d instance segmentation and tracking with voxel embedding based deep learning," in *MLMI*, 2021. 7
- [160] H.-Y. Meng, L. Gao, Y.-K. Lai, and D. Manocha, "Vv-net: Voxel vae net with group convolutions for point cloud segmentation," in *ICCV*, 2019. 7
- [161] A. B. L. Larsen, S. K. Sønderby, H. Larochelle, and O. Winther, "Autoencoding beyond pixels using a learned similarity metric," in *ICML*, 2016. 7
- [162] J. Li, C. Niu, and K. Xu, "Learning part generation and assembly for structure-aware shape synthesis," in *AAAI*, 2020. 7
- [163] M. Ibing, G. Kobsik, and L. Kobbelt, "Octree transformer: Autoregressive 3d shape generation on hierarchically structured sequences," *arXiv preprint arXiv:2111.12480*, 2021. 8
- [164] C. Xie, C. Wang, B. Zhang, H. Yang, D. Chen, and F. Wen, "Style-based point generator with adversarial rendering for point cloud completion," in *CVPR*, 2021. 8
- [165] L. Zhou, Y. Du, and J. Wu, "3d shape generation and completion through point-voxel diffusion," in *ICCV*, 2021. 9
- [166] R. Gal, A. Bermanno, H. Zhang, and D. Cohen-Or, "Mrgan: Multi-rooted 3d shape generation with unsupervised part disentanglement," in *ICCVW*, 2020. 9, 15
- [167] A. Zadeh, Y.-C. Lim, P. P. Liang, and L.-P. Morency, "Variational auto-decoder: A method for neural generative modeling from incomplete data," *arXiv preprint arXiv:1903.00840*, 2019. 9
- [168] X. Chen, T. Jiang, J. Song, J. Yang, M. J. Black, A. Geiger, and O. Hilliges, "gdna: Towards generative detailed neural avatars," in *CVPR*, 2022. 9, 14
- [169] M. Arjovsky and L. Bottou, "Towards principled methods for training generative adversarial networks," *arXiv preprint arXiv:1701.04862*, 2017. 10
- [170] A. Luo, T. Li, W.-H. Zhang, and T. S. Lee, "Surfgen: Adversarial 3d shape synthesis with explicit surface discriminators," in *ICCV*, 2021. 10
- [171] W. E. Lorensen and H. E. Cline, "Marching cubes: A high resolution 3d surface construction algorithm," *SIGGRAPH*, 1987. 10
- [172] E. Dupont, H. Kim, S. Eslami, D. Rezende, and D. Rosenbaum, "From data to functa: Your data point is a function and you should treat it like one," in *ICML*, 2022. 10
- [173] J.-Y. Zhu, Z. Zhang, C. Zhang, J. Wu, A. Torralba, J. Tenenbaum, and B. Freeman, "Visual object networks: Image generation with disentangled 3d representations," *NeurIPS*, 2018. 11, 12
- [174] X. Sun, J. Wu, X. Zhang, Z. Zhang, C. Zhang, T. Xue, J. B. Tenenbaum, and W. T. Freeman, "Pix3d: Dataset and methods for single-image 3d shape modeling," in *CVPR*, 2018. 11
- [175] P. Paysan, R. Knothe, B. Amberg, S. Romdhani, and T. Vetter, "A 3d face model for pose and illumination invariant face recognition," in *2009 sixth IEEE international conference on advanced video and signal based surveillance*, 2009. 11
- [176] Z. Liu, P. Luo, X. Wang, and X. Tang, "Deep learning face attributes in the wild," in *ICCV*, 2015. 11
- [177] W. Zhang, J. Sun, and X. Tang, "Cat head detection-how to effectively exploit shape and texture features," in *ECCV*, 2008. 11
- [178] L. Yang, P. Luo, C. Change Loy, and X. Tang, "A large-scale car dataset for fine-grained categorization and verification," in *CVPR*, 2015. 11
- [179] F. Yu, A. Seff, Y. Zhang, S. Song, T. Funkhouser, and J. Xiao, "Lsun: Construction of a large-scale image dataset using deep learning with humans in the loop," *arXiv preprint arXiv:1506.03365*, 2015. 11
- [180] T. H. Nguyen-Phuoc, C. Richardt, L. Mai, Y. Yang, and N. Mitra, "Blockgan: Learning 3d object-aware scene representations from unlabelled images," *NeurIPS*, 2020. 11, 12, 15
- [181] J. Johnson, B. Hariharan, L. Van Der Maaten, L. Fei-Fei, C. Lawrence Zitnick, and R. Girshick, "Clevr: A diagnostic dataset for compositional language and elementary visual reasoning," in *CVPR*, 2017. 11
- [182] X. Wang and A. Gupta, "Generative image modeling using style and structure adversarial networks," in *ECCV*, 2016. 11, 12
- [183] N. Silberman, D. Hoiem, P. Kohli, and R. Fergus, "Indoor segmentation and support inference from rgb-d images," in *ECCV*, 2012. 11
- [184] A. Noguchi and T. Harada, "Rgb-d-gan: Unsupervised 3d representation learning from natural image datasets via rgb-d image synthesis," *arXiv preprint arXiv:1909.12573*, 2019. 11
- [185] J. Krause, M. Stark, J. Deng, and L. Fei-Fei, "3d object representations for fine-grained categorization," in *ICCVW*, 2013. 11
- [186] Z. Shi, Y. Shen, J. Zhu, D.-Y. Yeung, and Q. Chen, "3d-aware indoor scene synthesis with depth priors," in *ECCV*, 2022. 11
- [187] A. Dosovitskiy, G. Ros, F. Codevilla, A. Lopez, and V. Koltun, "Carla: An open urban driving simulator," in *CORL*, 2017. 11
- [188] C. Wah, S. Branson, P. Welinder, P. Perona, and S. Belongie, "The caltech-ucsd birds-200-2011 dataset," California Institute of Technology, Tech. Rep., 2011. 11
- [189] K. Park, K. Rematas, A. Farhadi, and S. M. Seitz, "Photoshape: Photorealistic materials for large-scale shape collections," *TOG*, 2018. 11
- [190] X. Pan, X. Xu, C. C. Loy, C. Theobalt, and B. Dai, "A shading-guided generative implicit model for shape-accurate 3d-aware image synthesis," *NeurIPS*, 2021. 11, 12
- [191] M. Niemeyer and A. Geiger, "Campari: Camera-aware decomposed generative neural radiance fields," in *3DV*, 2021. 11, 13
- [192] P. Zhou, L. Xie, B. Ni, and Q. Tian, "Cips-3d: A 3d-aware generator of gans based on conditionally-independent pixel synthesis," *arXiv preprint arXiv:2110.09788*, 2021. 11, 13
- [193] Y. Choi, Y. Uh, J. Yoo, and J.-W. Ha, "Stargan v2: Diverse image synthesis for multiple domains," in *CVPR*, 2020. 11
- [194] X. Xu, X. Pan, D. Lin, and B. Dai, "Generative occupancy fields for 3d surface-aware image synthesis," *NeurIPS*, 2021. 11, 12, 15
- [195] J. Zhang, E. Sangineto, H. Tang, A. Siarohin, Z. Zhong, N. Sebe, and W. Wang, "3d-aware semantic-guided generative model for human synthesis," in *ECCV*, 2022. 11, 13
- [196] Z. Liu, P. Luo, S. Qiu, X. Wang, and X. Tang, "Deepfashion: Powering robust clothes recognition and retrieval with rich annotations," in *CVPR*, 2016. 11
- [197] J. Sun, X. Wang, Y. Zhang, X. Li, Q. Zhang, Y. Liu, and J. Wang, "Fenerf: Face editing in neural radiance fields," in *CVPR*, 2022. 11, 13, 15
- [198] C.-H. Lee, Z. Liu, L. Wu, and P. Luo, "Maskgan: Towards diverse and interactive facial image manipulation," in *CVPR*, 2020. 11
- [199] J. Gu, L. Liu, P. Wang, and C. Theobalt, "Stylenerf: A style-based 3d-aware generator for high-resolution image synthesis," in *ICLR*, 2022. 11, 13, 14, 15
- [200] T. Karras, M. Aittala, J. Hellsten, S. Laine, J. Lehtinen, and T. Aila, "Training generative adversarial networks with limited data," *NeurIPS*, 2020. 11
- [201] R. Or-El, X. Luo, M. Shan, E. Shechtman, J. J. Park, and I. Kelmenacher-Shlizerman, "Style3d: High-resolution 3d-consistent image and geometry generation," in *CVPR*, 2022. 11, 13, 15
- [202] Y. Deng, J. Yang, J. Xiang, and X. Tong, "Gram: Generative radiance manifolds for 3d-aware image generation," in *CVPR*, 2022. 11, 13, 15
- [203] F. Tan, S. Fanello, A. Meka, S. Orts-Escobedo, D. Tang, R. Pandey, J. Taylor, P. Tan, and Y. Zhang, "Volux-gan: A generative model for 3d face synthesis with hdri relighting," *TOG*, 2022. 11, 13, 14, 15
- [204] Y. Xue, Y. Li, K. K. Singh, and Y. J. Lee, "Giraffe hd: A high-resolution 3d-aware generative model," in *CVPR*, 2022. 11, 13
- [205] X. Zhang, Z. Zheng, D. Gao, B. Zhang, P. Pan, and Y. Yang, "Multi-view consistent generative adversarial networks for 3d-aware image synthesis," in *CVPR*, 2022. 11, 13
- [206] A. Noguchi, X. Sun, S. Lin, and T. Harada, "Unsupervised learning of efficient geometry-aware neural articulated representations," in *ECCV*, 2022. 11, 15
- [207] S. Peng, Y. Zhang, Y. Xu, Q. Wang, Q. Shuai, H. Bao, and X. Zhou, "Neural body: Implicit neural representations with structured latent codes for novel view synthesis of dynamic humans," in *CVPR*, 2021. 11

- [208] G. Varol, J. Romero, X. Martin, N. Mahmood, M. J. Black, I. Laptev, and C. Schmid, "Learning from synthetic humans," in *CVPR*, 2017. **11**
- [209] R. Li, S. Yang, D. A. Ross, and A. Kanazawa, "Ai choreographer: Music conditioned 3d dance generation with aist++," in *ICCV*, 2021. **11**
- [210] T.-Y. Lin, M. Maire, S. Belongie, J. Hays, P. Perona, D. Ramanan, P. Dollár, and C. L. Zitnick, "Microsoft coco: Common objects in context," in *ECCV*, 2014. **11**
- [211] J. Sun, X. Wang, Y. Shi, L. Wang, J. Wang, and Y. Liu, "Ide-3d: Interactive disentangled editing for high-resolution 3d-aware portrait synthesis," in *SIGGRAPH Asia*, 2022. **11, 13, 14, 15**
- [212] I. Skorokhodov, S. Tulyakov, Y. Wang, and P. Wonka, "Epigraf: Rethinking training of 3d gans," *arXiv preprint arXiv:2206.10535*, 2022. **11**
- [213] J. Zhang, Z. Jiang, D. Yang, H. Xu, Y. Shi, G. Song, Z. Xu, X. Wang, and J. Feng, "Avatargen: a 3d generative model for animatable human avatars," *arXiv preprint arXiv:2208.00561*, 2022. **11, 14, 15**
- [214] H. Dong, X. Liang, X. Shen, B. Wang, H. Lai, J. Zhu, Z. Hu, and J. Yin, "Towards multi-pose guided virtual try-on network," in *ICCV*, 2019. **11**
- [215] P. Zablotskaia, A. Siarohin, B. Zhao, and L. Sigal, "Dwnet: Dense warp-based network for pose-guided human video generation," *arXiv preprint arXiv:1910.09139*, 2019. **11**
- [216] L. Gao, J. Yang, T. Wu, Y.-J. Yuan, H. Fu, Y.-K. Lai, and H. Zhang, "Sdm-net: Deep generative network for structured deformable mesh," *TOG*, 2019. **10**
- [217] Y. Shen, J. Gu, X. Tang, and B. Zhou, "Interpreting the latent space of gans for semantic face editing," in *CVPR*, 2020. **10**
- [218] A. Tewari, M. Elgharib, G. Bharaj, F. Bernard, H.-P. Seidel, P. Pérez, M. Zollhofer, and C. Theobalt, "Stylrig: Rigging stylegan for 3d control over portrait images," in *CVPR*, 2020. **10**
- [219] Y. Deng, J. Yang, D. Chen, F. Wen, and X. Tong, "Disentangled and controllable face image generation via 3d imitative-contrastive learning," in *CVPR*, 2020. **10**
- [220] C. Yang, Y. Shen, and B. Zhou, "Semantic hierarchy emerges in deep generative representations for scene synthesis," *IJCV*, 2021. **10**
- [221] T. Leimkühler and G. Drettakis, "Freestylegan: Free-view editable portrait rendering with the camera manifold," *arXiv preprint arXiv:2109.09378*, 2021. **10**
- [222] M. Mirza and S. Osindero, "Conditional generative adversarial nets," *arXiv preprint arXiv:1411.1784*, 2014. **11**
- [223] V. Sitzmann, M. Zollhöfer, and G. Wetzstein, "Scene representation networks: Continuous 3d-structure-aware neural scene representations," in *NeurIPS*, 2019. **12**
- [224] X. Chen, D. Cohen-Or, B. Chen, and N. J. Mitra, "Towards a neural graphics pipeline for controllable image generation," in *CGF*, 2021. **12**
- [225] P. Henzler, N. J. Mitra, and T. Ritschel, "Escaping plato's cave: 3d shape from adversarial rendering," in *ICCV*, 2019. **12**
- [226] V. Sitzmann, J. Martel, A. Bergman, D. Lindell, and G. Wetzstein, "Implicit neural representations with periodic activation functions," *NeurIPS*, 2020. **12**
- [227] E. Perez, F. Strub, H. De Vries, V. Dumoulin, and A. Courville, "Film: Visual reasoning with a general conditioning layer," in *AAAI*, 2018. **12**
- [228] V. Dumoulin, E. Perez, N. Schucher, F. Strub, H. d. Vries, A. Courville, and Y. Bengio, "Feature-wise transformations," *Distill*, 2018. **12**
- [229] Z. Shi, Y. Xu, Y. Shen, D. Zhao, Q. Chen, and D.-Y. Yeung, "Improving 3d-aware image synthesis with a geometry-aware discriminator," in *NeurIPS*, 2022. **13**
- [230] J. Xiang, J. Yang, Y. Deng, and X. Tong, "Gram-hd: 3d-consistent image generation at high resolution with generative radiance manifolds," *arXiv preprint arXiv:2206.07255*, 2022. **13**
- [231] I. Skorokhodov, S. Tulyakov, Y. Wang, and P. Wonka, "Epigraf: Rethinking training of 3d gans," *arXiv preprint arXiv:2206.10535*, 2022. **13**
- [232] T. DeVries, M. A. Bautista, N. Srivastava, G. W. Taylor, and J. M. Susskind, "Unconstrained scene generation with locally conditioned radiance fields," in *ICCV*, 2021. **13**
- [233] Z. Hao, A. Mallya, S. Belongie, and M.-Y. Liu, "Gancraft: Unsupervised 3d neural rendering of minecraft worlds," in *ICCV*, 2021. **13**
- [234] R. Abdal, Y. Qin, and P. Wonka, "Image2stylegan: How to embed images into the stylegan latent space?" in *ICCV*, 2019. **13**
- [235] S. Pidhorskyi, D. Adjeroh, and G. Doretto, "Adversarial latent autoencoders," in *CVPR*, 2020. **13**
- [236] S. Cai, A. Obukhov, D. Dai, and L. Van Gool, "Pix2nerf: Unsupervised conditional p-gan for single image to neural radiance fields translation," in *CVPR*, 2022. **13**
- [237] A. Tewari, X. Pan, O. Fried, M. Agrawala, C. Theobalt *et al.*, "Disentangled3d: Learning a 3d generative model with disentangled geometry and appearance from monocular images," in *CVPR*, 2022. **13, 15**
- [238] M. Lee, C. Chung, H. Cho, M. Kim, S. Jung, J. Choo, and M. Sung, "3d-gif: 3d-controllable object generation via implicit factorized representations," *arXiv preprint arXiv:2203.06457*, 2022. **13, 15**
- [239] A. R. Kosiorek, H. Strathmann, D. Zoran, P. Moreno, R. Schneider, S. Mokrá, and D. J. Rezende, "Nerf-vae: A geometry aware 3d scene generative model," in *ICML*, 2021. **13**
- [240] D. Rebain, M. J. Matthews, K. M. Yi, D. Lagun, and A. Tagliasacchi, "Lolnerf: Learn from one look," in *CVPR*, 2022. **13**
- [241] J. Gao, T. Shen, Z. Wang, W. Chen, K. Yin, D. Li, O. Litany, Z. Gojcic, and S. Fidler, "GET3D: A generative model of high quality 3d textured shapes learned from images," in *NeurIPS*, 2022. **14**
- [242] A. W. Bergman, P. Kellnhofer, Y. Wang, E. R. Chan, D. B. Lindell, and G. Wetzstein, "Generative neural articulated radiance fields," *arXiv preprint arXiv:2206.14314*, 2022. **14, 15**
- [243] Y. Yuan, Y. Lai, T. Wu, L. Gao, and L. Liu, "A revisit of shape editing techniques: From the geometric to the neural viewpoint," *JCST*, 2021. **14**
- [244] J. Liu, F. Yu, and T. A. Funkhouser, "Interactive 3d modeling with a generative adversarial network," in *3DV*, 2017. **14**
- [245] Z. Zheng, T. Yu, Q. Dai, and Y. Liu, "Deep implicit templates for 3d shape representation," in *CVPR*, 2021. **14**
- [246] T. Jahan, Y. Guan, and O. van Kaick, "Semantics-guided latent space exploration for shape generation," *CGF*, 2021. **15**
- [247] Z. Liu, Y. Wang, X. Qi, and C. Fu, "Towards implicit text-guided 3d shape generation," *CVPR*, 2022. **15**
- [248] R. Fu, X. Zhan, Y. Chen, D. Ritchie, and S. Sridhar, "Shapecrafter: A recursive text-conditioned 3d shape generation model," *arXiv preprint arXiv:2207.09446*, 2022. **15**
- [249] Y. Liao, K. Schwarz, L. M. Mescheder, and A. Geiger, "Towards unsupervised learning of generative models for 3d controllable image synthesis," in *CVPR*, 2020. **15**
- [250] C. Wang, M. Chai, M. He, D. Chen, and J. Liao, "Clip-nerf: Text-and-image driven manipulation of neural radiance fields," *CVPR*, 2022. **15**
- [251] B. Zhang, M. Nießner, and P. Wonka, "3dilg: Irregular latent grids for 3d generative modeling," *arXiv preprint arXiv:2205.13914*, 2022. **15**
- [252] S. Duggal, Z. Wang, W. Ma, S. Manivasagam, J. Liang, S. Wang, and R. Urtasun, "Secrets of 3d implicit object shape reconstruction in the wild," *arXiv preprint arXiv:2101.06860*, 2021. **15**
- [253] A. Yuille and D. Kersten, "Vision as bayesian inference: analysis by synthesis?" *Trends in Cognitive Sciences*, 2006. **15**
- [254] X. Chen, Z. Dong, J. Song, A. Geiger, and O. Hilliges, "Category level object pose estimation via neural analysis-by-synthesis," in *ECCV*, 2020. **15**
- [255] J. Guo, F. Zhong, R. Xiong, Y. Liu, Y. Wang, and Y. Liao, "A visual navigation perspective for category-level object pose estimation," in *ECCV*, 2022. **15**
- [256] B. Eckart, W. Yuan, C. Liu, and J. Kautz, "Self-supervised learning on 3d point clouds by learning discrete generative models," in *CVPR*, 2021. **15**
- [257] A. Ramesh, P. Dhariwal, A. Nichol, C. Chu, and M. Chen, "Hierarchical text-conditional image generation with CLIP latents," *arXiv preprint arXiv:2204.06125*, 2022. **15**
- [258] C. Saharia, W. Chan, S. Saxena, L. Li, J. Whang, E. Denton, S. K. S. Ghasemipour, B. K. Ayan, S. S. Mahdavi, R. G. Lopes, T. Salimans, J. Ho, D. J. Fleet, and M. Norouzi, "Photorealistic text-to-image diffusion models with deep language understanding," *arXiv preprint arXiv:2205.11487*, 2022. **15**
- [259] A. Liu, A. Makadia, R. Tucker, N. Snavely, V. Jampani, and A. Kanazawa, "Infinite nature: Perpetual view generation of natural scenes from a single image," in *ICCV*, 2021. **15**